How to kill bacteria

fast

and slow

A thesis submitted to attain the degree of

DOCTOR OF SCIENCES of ETH ZURICH

(Dr. sc. ETH Zurich)

presented by

MALTE MÜTTER

MSc., TU Berlin

born on December 1st, 1992

accepted on the recommendation of

Prof. Dr. Sebastian Bonhoeffer, ETH Zürich

Prof. Dr. Roland Regoes

Dr. Danie Angst

2025

Summary

Since the discovery of penicillin, antibiotics have been a cornerstone of modern medicine, saving countless lives. This achievement is now under threat, as bacteria have evolved resistance mechanisms against most available drugs. Resistance arises through the acquisition of resistance genes—either via mutations or through horizontal transfer on mobile genetic elements such as plasmids—and is selected for according to the administered drugs, their concentrations, and the pharmacodynamics that link treatment to its effect on the bacterial population.

To curb the spread of resistance, antibiotics should ideally be chosen on the basis of phenotypic information. In emergency situations, however, this is not always feasible. Therapy then relies on predefined treatment protocols rather than tailored data. Chapter 2 examines how these default protocols (treatment strategies) influence the persistence of plasmid-mediated resistance and the emergence of new double resistance. We performed large-scale automated in-vitro experiments that mimic hospital-like transmission dynamics, using two antibiotics in combination with two resistance plasmids derived from clinical isolates.

We found that administering both drugs to every patient (combination therapy) was the most effective strategy in most scenarios. Although theoretical models often predict the success of combination therapy, the clinical literature is less conclusive. This gap has several causes: some drug pairs act synergistically, whereby the combined effect exceeds the sum of single-drug effects, whereas others act antagonistically, reducing overall efficacy.

Drug interactions have so far been studied mainly at concentrations below the minimal inhibitory concentration (MIC), where growth can be tracked conveniently by optical density (OD). OD cannot measure bacterial decline, and probing the clinically relevant super-MIC range—where bacteria are actively killed—requires colony-forming-unit (CFU) assays, which are labor-intensive and unsuited to high throughput.

Chapter 3 therefore evaluates whether a luminescence-based high-throughput method, previously validated for sub-MIC conditions, can also track population dynamics across the entire concentration range. Using bacteria engineered to emit bioluminescent light, we show that this method accurately estimates net growth rates for drugs that do not induce significant filamentation.

Building on these insights, Chapter 4 explores drug interactions for six antibiotics that performed well in the preceding validation. We analysed 15 drug pairs across 144 concentration combinations each, introducing a mathematical framework to describe the pharmacodynamics of combinations. By comparing observed effects to null models of non-interaction, we classified pairs as neutral, synergistic or antagonistic, and demonstrated that interaction types can shift markedly between sub- and super-MIC conditions.

Together, these studies combine experimental and theoretical approaches to elucidate antibiotic effects on bacterial populations and resistance evolution. They deliver robust tools for quantifying population dynamics and bolster the case for combination therapy, while refining our understanding of drug–drug interactions across clinically relevant concentration ranges.

Zusammenfassung

Seit der Entdeckung des Penicillins bilden Antibiotika einen Grundpfeiler der modernen Medizin und haben unzählige Leben gerettet. Dieser Erfolg ist jedoch bedroht, da Bakterien gegen die meisten verfügbaren Wirkstoffe Resistenzmechanismen entwickelt haben. Resistenzen entstehen durch den Erwerb von Resistenzgenen – entweder über Mutationen oder durch horizontalen Gentransfer via mobile genetische Elemente wie Plasmide – und werden abhängig von verabreichten Wirkstoffen, deren Konzentrationen und den Pharmakodynamiken selektiert, die Behandlung und Wirkung miteinander verknüpfen.

Um die Ausbreitung von Resistenzen einzudämmen, sollten Antibiotika idealerweise auf Basis phänotypischer Informationen ausgewählt werden. In Notfallsituationen ist dies jedoch oft nicht möglich, sodass auf vordefinierte Behandlungsprotokolle zurückgegriffen wird. Kapitel 2 untersucht, wie diese Standardprotokolle (Behandlungsstrategien) die Persistenz plasmidvermittelter Resistenzen und das Auftreten neuer Doppelresistenzen beeinflussen. Hierfür führten wir groß angelegte, automatisierte In-vitro-Experimente durch, die krankenhausähnliche Übertragungsdynamiken simulieren; zum Einsatz kamen zwei Antibiotika in Kombination mit zwei aus klinischen Isolaten stammenden Resistenzplasmiden.

Die Gabe beider Wirkstoffe an jeden Patienten (Kombinationstherapie) erwies sich in den meisten Szenarien als wirksamste Strategie. Obwohl theoretische Modelle diesen Erfolg häufig vorhersagen, ist die klinische Datenlage weniger eindeutig. Ursachen hierfür sind unter anderem synergistische Wirkstoffpaarungen, bei denen der kombinierte Effekt größer ist als die Summe der Einzeleffekte, sowie antagonistische Paarungen, bei denen er kleiner ausfällt.

Bisher wurden Arzneimittelinteraktionen überwiegend bei Konzentrationen unterhalb der minimalen Hemmkonzentration (MIC) untersucht, da Wachstumsraten dort bequem mittels optischer Dichte (OD) erfassbar sind. OD misst jedoch keinen Bakterienrückgang. Der klinisch relevante Super-MIC-Bereich, in dem Bakterien aktiv abgetötet werden, erfordert koloniebildende Einheiten (CFU), ein arbeitsintensives und wenig durchsatzstarkes Verfahren.

Kapitel 3 prüft daher, ob eine bereits für Sub-MIC-Bedingungen validierte, lumineszenzbasierte Hochdurchsatzmethode auch über den gesamten Konzentrationsbereich einsetzbar ist. Durch gentechnisch veränderte, bioluminezente Bakterien konnten wir zeigen, dass diese Methode die Nettowachstumsrate für Wirkstoffe ohne ausgeprägte Filamentierung präzise erfasst.

Aufbauend darauf untersucht Kapitel 4 Wirkstoffinteraktionen für sechs im Vorversuch bewährte Antibiotika. Wir analysierten 15 Wirkstoffpaare mit jeweils 144 Konzentrationskombinationen und entwickelten einen mathematischen Rahmen zur Beschreibung der Pharmakodynamik von Kombinationen. Durch Vergleich der beobachteten Effekte mit Nullmodellen ohne Interaktion klassifizierten wir Paare als neutral, synergistisch oder antagonistisch und zeigten, dass sich diese Klassifikationen zwischen Sub- und Super-MIC-Bereichen deutlich ändern können.

Insgesamt verbinden diese Arbeiten experimentelle und theoretische Ansätze, um die Wirkung von Antibiotika auf bakterielle Populationen und die Resistenzentwicklung zu beleuchten. Sie liefern robuste Methoden zur Quantifizierung von Populationsdynamiken, stärken die Evidenz

für Kombinationstherapien und verfeinern unser Verständnis von Arzneimittelinteraktionen über klinisch relevante Konzentrationsbereiche hinweg.

Preface

about data and stuff...

Bibliography

CONTENTS

Summary i

Zusammenfassung iii

1 introduction 1
1.1 Thesis outline 4

2 The Impact of Treatment Strategies on the Epidemiological Dynamics of Plasmid-Conferred Antibiotic Resistance 7
2.1 abstract 7
2.2 Introduction 7
2.3 Results 10
2.4 Discussion 17
2.5 Methods 21
2.6 Supplementary Information 27

3 Concluding Remarks 65
3.1 Is combination the best treatment strategy? 65
3.2 Can we use change of luminescent light intensity to approximate the net growth rate? 65
3.3 can we extrapolate sub-mic measures of drug interactions to the super-mic? . . . 65
3.4 General Concluding Note 65

1. format frontpage for papers. Do it like niko. Abstract; Authors; Contributions; and manuscript accepted/submitted/in preparation.

2. improve formatting of chapter and section titles

1 Introduction

Antibiotics have nearly eliminated premature death from bacterial infections in most parts of the developed world, to the extent that effective treatment is now often taken for granted [Hawkey2008]. The threat to this achievement posed by antibiotic resistance was recognized early, for instance by Kirby (1944), and explicitly highlighted by Alexander Fleming in his 1945 Nobel Prize speech. Today, this threat has materialized: antimicrobial resistance (AMR) contributed to an estimated 4.71 million deaths in 2021, with 1.14 million deaths directly attributable to resistant infections [1]. The possibility of returning to a world where antibiotics are largely ineffective underscores the importance of understanding the ecological and evolutionary forces shaping AMR.

Evolution of antibiotic resistance is driven by two key processes: mutation and selection. Resistance genes arise de novo through mutations, occurring either on bacterial chromosomes or on extrachromosomal mobile genetic elements that replicate independently, such as plasmids (small circular DNA molecules) or bacteriophages (viruses targeting bacteria). Once established, these genes can spread.

Resistance genes spread in two fundamentally different ways: vertically, when a mother cell passes them to its progeny during division, and horizontally, when previously susceptible bacteria acquire foreign DNA. Horizontal transfer is often mediated by plasmids, many of which can actively initiate their own conjugation by assembling a pilus — a physical tunnel connecting donor and recipient cells — through which plasmid DNA is delivered. However, not all plasmids initiate conjugation: some rely exclusively on vertical inheritance, while others lack conjugation machinery but can opportunistically transfer by exploiting the conjugation apparatus of co-resident plasmids. Plasmid conjugation can facilitates gene exchange across bacterial lineages and even species boundaries [Frost2005, Smillie2010].

Whether these emerged resistance genes can persist depends on selection. Selection is shaped by the interplay between (i) pharmacokinetics (PK), which describes how drug concentrations

change over time within the host, and (ii) pharmacodynamics (PD), which describes how these concentrations influence bacterial population dynamics [2].

Each use of antibiotics imposes selective pressure on microbial populations, which can favor the emergence or spread of resistant variants. This is consistent with the widely accepted view that antibiotic use is the main driver of resistance evolution [Gregory2018]. However, because infections can be life-threatening, antibiotic use is often unavoidable, creating a trade-off between effective treatment and the risk of selecting for resistant bacteria.

This raises the fundamental question of how to best use antibiotics to treat infections; with and without knowledge about the phenotypic properties of the infecting pathogen. Furthermore, this question arises at multiple biological scales: within individual hosts, where antibiotic concentrations and bacterial populations interact dynamically; and between hosts, where treatment strategies influence the transmission and spread of resistance at the population level. Both scales are relevant for evaluating the effectiveness and evolutionary consequences of antibiotic use.

Treatment Strategies and Combination Therapy

In an ideal scenario, the treatment of infections is tailored to the resistance phenotype of the infecting pathogen. However, in clinical practice this is often not feasible: in emergency settings, immediate treatment is required and microbiological characterisation typically takes 24 to 72 hours [Leekha2011]; resistance may exist below detection thresholds, rendering diagnostics inconclusive; and in prophylactic contexts such as surgery or treatment of immunocompromised patients, antibiotics are often prescribed preemptively.

In such cases of limited information, clinicians rely on empirical treatment strategies that aim to minimize the risk of selecting for resistance. Commonly discussed approaches include combination therapy (simultaneous use of multiple antibiotics), mixing (random patient allocation to different antibiotics), and cycling (periodic rotation of antibiotics over time). Among these, combination therapy, which was first introduced in agriculture to prevent resistance in plant pathogens [3–5] is often considered the most promising strategy in theoretical models [6–8].

However, concerns persist. One major concern is that combination therapy might accelerate the selection for resistance, given the observed correlation between overall antibiotic consumption and resistance [gregory], not only regarding the targeted pathogen but also for the microbiome [...].

Furthermore, combining antibiotics may impose a higher burden on patients, for example through an increased risk of toxicity [9].

In the clinical context combination therapy plays a central role in clinical protocols for rapidly evolving pathogens such as HIV, Mycobacterium tuberculosis, and Plasmodium falciparum [10]. Nonetheless, the clinical evidence remains inconclusive. A recent meta-analysis found no consistent advantage of combination therapy in preventing resistance across bacterial infections [11]. The discrepancy between theoretical predictions and inconclusive clinical outcomes can stem both from limitations in modelling or clinical study design. On the theoretical side, models often rely on simplifying assumptions and may overlook important biological complexities, such as heterogeneity in patients, pathogens, and treatment responses. On the clinical side, most trials are not designed to detect resistance outcomes and are therefore underpowered for this purpose [11]. Additional variability arises from differences in study design, pathogens, treatment regimens, and clinical endpoints. Moreover, the choice of antibiotic combination itself can increase or decrease treatment success, further contributing to outcome variability.

To bridge the gap between theoretical models and clinical studies, Angst et al. [12] developed an in vitro experimental setup mimicking within- and between-host dynamics under different treatment strategies, and showing that combination therapy typically best prevents resistance emergence best.

In Chapter 2, we refine this framework to study plasmid-mediated resistance. Our results confirmed that combination therapy remains the most effective strategy in most scenarios.

Population Dynamics under Combination Therapy

To better understand the potential of combination therapy, a deeper insight into drug interactions is needed. Drug interaction studies evaluate how the combined effect of two antibiotics compares to a predicted neutral effect derived from their individual actions. Two classical null models are typically used for this purpose: the Loewe additivity model [13] and the Bliss independence model [Bliss1939]. Numerous studies have investigated drug interactions below the minimum inhibitory concentration (MIC) [14], ([...]) providing valuable insights into sublethal interactions. However, it remains unclear whether these findings extend to the super-MIC range, where antibiotics are expected to kill bacteria. This uncertainty arises from the scarcity of studies

exploring interactions above the MIC.

The reason for this is methodological: to quantify treatment effects, we estimate the exponential change in time-series population curves. Below the MIC, bacterial growth is typically quantified using optical density (OD), which allows for high-throughput measurement. However, OD does not distinguish between live and dead cells, making it unreliable for estimating net growth rates above the MIC. At super-MIC concentrations, colony-forming unit (CFU) assays remain the gold standard, but they are labor-intensive, costly, and can become unreliable at high drug levels.

To address this gap, Chapter 3 evaluates luminescence as a high-throughput alternative to CFU counting and tests how reliably each method captures bacterial dynamics at inhibitory drug levels. We find that luminescence assays tend to track biomass more closely than viable cell numbers; which can cause divergence for estimated rates when cells filament.

Using this validated approach, Chapter 4 systematically characterizes pharmacodynamic interactions for multiple antibiotic pairs, examining whether interaction classifications are consistent across sub- and super-MIC concentration ranges.

1.1 Thesis outline

In this thesis we develop experimental and analytical methods to quantify how antibiotic-induced selection pressure shapes the evolution and transmission of resistance at both within-host and between-host scales.

In Chapter 2, we use an in-vitro hospital-ward model, to compare three multidrug strategies (combination, mixing, cycling), two monotherapies (Mono A, Mono B) and an untreated control. We show that combination therapy suppresses plasmid-borne double resistance most efficiently under the majority of conditions, but also find that in certain scenarios, mixing, cycling, or even monotherapy can perform equally well. Surprisingly, we find that omitting treatment entirely can accelerate the emergence of multi-resistance—a phenomenon specific to plasmid-mediated resistance dynamics.

In Chapter 3, we assess the applicability of luminescence assays as a high-throughput method for estimating net growth above the MIC, benchmark them against CFU counts, and develop a mathematical framework that explains when each read-out reflects biomass, viable cell number, or neither. We find that light intensity correlates more closely with biomass than with viable

cell number, which leads to discrepancies in growth-rate estimates under conditions that induce filamentation. However, we encountered two well-documented yet commonly ignored limitations of CFU counting — antibiotic carry-over and loss of culturability —– which make rate estimates unreliable at high drug concentrations.

In Chapter 4, we build on the validated luminescence workflow, and use it to map net-growth surfaces for 2160 drug–drug–concentration combinations, using six antibiotics. From these data, we derive interaction parameters for each pair and compare them to the expectations under Loewe additivity and Bliss independence. We find that the classification of drug interactions can shift between sub- and super-MIC ranges, implying that interaction types at sub-MIC levels do not necessarily generalise to inhibitory concentrations. Furthermore, we extend the pharmacodynamic formalism to be applicable for drug combinations, allowing us to analyse how pharmacodynamic parameters of individual drugs combine under co-treatment.

We conclude the thesis in Chapter 5 with a synthesis of our findings and a discussion of their implications for optimising antibiotic use.

Bibliography

[1] .M. Naghavi et al. “Global burden of bacterial antimicrobial resistance 1990–2021: a systematic analysis with forecasts to 2050”. In: Lancet 404.10459 (Sept. 2024), pp. 1199–1226. issn: 1474547X. doi: 10.1016/S0140-6736(24)01867-1/ATTACHMENT/4F9FA746-A486-4BC0-BF71-075D4D1D6D56/MMC3.PDF. url: https://www.thelancet.com/action/showFullText?pii=S0140673624018671%20https://www.thelancet.com/action/showAbstract?pii=S0140673624018671%20https://www.thelancet.com/journals/lancet/article/PIIS0140-6736(24)01867-1/abstract.

[2] .R. R. Regoes, C. Wiuff, R. M. Zappala, K. N. Garner, F. Baquero, and B. R. Levin. “Pharmacodynamic functions: A multiparameter approach to the design of antibiotic treatment regimens”. In: Antimicrob. Agents Chemother. 48.10 (2004), pp. 3670–3676. issn: 00664804. doi: 10.1128/AAC.48.10.3670-3676.2004.

[3] .P. F. Kable and H. Jeffery. “Selection for Tolerance in Organisms Exposed to Sprays of Biocide Mixtures: A Theoretical Model”. In: Phytopathology 70.1 (1980), pp. 8–12. issn: 0031-949X. doi: 10.1094/phyto-70-8.

[4] .C. J. Delp. “Coping with resistance to plant disease”. In: Plant Dis. 64 (1980), pp. 652–657. doi: 10.1094/PD-64-652.

[5] .G. Skylakakis. “Effects of Alternating and Mixing Pesticides on the Buildup of Fungal Resistance”. In: Phytopathology 71.11 (1981), pp. 1119–1121. issn: 0031-949X. doi: 10.1094/phyto-71-1119.

[6] .S. Bonhoeffer, M. Lipsitch, and B. R. Levin. “Evaluating treatment protocols to prevent antibiotic resistance”. In: Proc. Natl. Acad. Sci. U. S. A. 94.22 (1997), pp. 12106–12111. issn: 00278424. doi: 10.1073/pnas.94.22.12106.

[7] .B. Tepekule, H. Uecker, I. Derungs, A. Frenoy, and S. Bonhoeffer. “Modeling antibiotic treatment in hospitals: A systematic approach shows benefits of combination therapy over cycling, mixing, and mono-drug therapies”. In: PLoS Comput. Biol. 13.9 (2017), pp. 1–22. issn: 15537358. doi: 10.1371/journal.pcbi.1005745.

[8] .H. Uecker and S. Bonhoeffer. “Antibiotic treatment protocols revisited: The challenges of a conclusive assessment by mathematical modelling”. In: J. R. Soc. Interface 18.181 (2021). issn: 17425662. doi: 10.1098/rsif.2021.0308.

[9] .P. D. Tamma, S. E. Cosgrove, and L. L. Maragakis. “Combination therapy for treatment of infections with gram-negative bacteria”. In: Clin. Microbiol. Rev. 25.3 (2012), pp. 450–470. issn: 08938512. doi: 10.1128/CMR.05041-11.

[10] .D. E. Goldberg, R. F. Siliciano, and W. R. Jacobs. “Outwitting evolution: Fighting drug-resistant TB, Malaria, and HIV”. In: Cell 148.6 (2012), pp. 1271–1283. issn: 10974172. doi: 10.1016/j.cell.2012.02.021.

[11] .B. Siedentop, V. N. Kachalov, C. Witzany, M. Egger, D. Roger, and S. Bonhoeffer. “The effect of combining antibiotics on resistance : A systematic review and meta-analysis”. In: Elife 13 (2024), pp. 1–25. doi: 10.7554/eLife.93740.1.

[12] .D. C. Angst, B. Tepekule, L. Sun, B. Bogos, and S. Bonhoeffer. “Comparing treatment strategies to reduce antibiotic resistance in an in vitro epidemiological setting”. In: Proc. Natl. Acad. Sci. U. S. A. 118.13 (2021), pp. 1–7. issn: 10916490. doi: 10.1073/PNAS.2023467118.

[13] .S. Loewe and M. H. “Über Kombinationswirkungen.” In: (1926).

[14] .P. Yeh, A. I. Tschumi, and R. Kishony. “Functional classification of drugs by properties of their pairwise interactions”. In: Nat. Genet. 38.4 (2006), pp. 489–494. issn: 10614036. doi: 10.1038/ng1755.

2 The Impact of Treatment Strategies on the Epidemiological Dynamics of Plasmid-Conferred Antibiotic Resistance

2.1 abstract

The issue of antibiotic resistance is a critical concern for public health, prompting numerous investigations into the impact of treatment strategies on preventing or slowing down the emergence of resistance. While existing studies have predominantly focused on chromosomal resistance mutations, the consequences of often clinically more relevant plasmid-conferred resistance remain insufficiently explored.

To address this gap, we conducted three extensive in vitro experiments utilising a liquid-handling platform. These experiments evaluated the efficacy of five distinct treatment strategies using two antibiotics (tetracycline and ceftazidime) along with two horizontally transmissible clinical resistance plasmids conferring the respective resistances.

Among the experimentally investigated treatment strategies, combination therapy proved to be the most effective in preventing the emergence of double resistance while minimising the number of infections.

To verify the reliability of these findings, we constructed a computational model of our experiments that we parameterised using the experimental data. We employed this model to augment the experimental data by conducting an in silico parameter sensitivity analysis. The sensitivity analysis corroborated our experimental results, demonstrating that combination therapy consistently outperformed other treatment strategies across a range of parameter values.

2.2 Introduction

In light of the growing threat of antimicrobial resistance (AMR) to human health, various multidrug strategies are being considered to improve the sustainability of antibiotic use. These approaches include combination therapy (simultaneous use of multiple antibiotics), mixing therapy

(randomly assigning patients to receive different antibiotics), and cycling therapy (alternating between multiple antibiotics over time).

Combination, originally proposed alongside cycling therapy to prevent biocide resistance in plant pathogens [1–3], was later adopted in human medicine. Combination therapy proved its effectiveness in preventing resistance evolution in highly adaptable pathogens such as HIV, Mycobacterium tuberculosis, and Plasmodium falciparum [4]. However, a recent meta-analysis investigating the effect of combination therapy on resistance across various bacterial infections and antibiotic combinations found no evidence for a difference in the risk of resistance acquisition [5]. Also, a comprehensive cluster-randomised crossover study comparing mixing and cycling by van Duijn et al. [6], spanning nearly two years across eight ICUs, found no significant differences in outcomes.

A review of the available model literature by Uecker et al. [7] reveals the complexity and context-dependent efficacy of treatment strategies such as combination, cycling or mixing strategies. Yet, theoretical models often identify combination therapy as the best strategy to prevent new resistance [8, 9]. It remains unclear whether the inconclusive results regarding the effectiveness of multidrug treatment strategies in the literature are due to the theoretical models failing to account for key processes, or if clinical studies lack statistical power, as suggested by Siedentop et al. [5]. This lack of power may be caused by patient and bacterial strain heterogeneity, stochasticity in infection dynamics, and other unknown factors that make it difficult to isolate single effects.

We recently started experiments to make a foray into the large gap between theoretical models and clinical trials. In an in vitro experiment mimicking the epidemiological scenario of transmission in a hospital ward, Angst et al. [10] investigated the effect of cycling, mixing, and combination therapy on resistance evolution and showed that for chromosomal resistance mutations combination therapy outperformed the other strategies. One potential reason why combination therapy succeeded in that study and tends to be superior in mathematical models is that it increases the genetic barrier to resistance by requiring the acquisition of multiple mutations in the same background.

Here, we explore the effect of horizontal gene transfer (HGT) on resistance evolution under treatment by conducting three large-scale in vitro experiments. The experiments mimic epi-

demiological transmission dynamics of symptomatic infections by a focal strain in an intensive care unit (ICU) and include patient discharge and admission, infection between patients, and treatment. We use two antibiotics, ceftazidime (A) and tetracycline (B), along with two clinical resistance plasmids [11] we call p_A and p_B, conferring resistance to the corresponding antibiotics. The plasmids are compatible, can conjugate, and were isolated from clinical samples collected and characterised in a study at University Hospital Basel [12]. We model patients as wells in a 384-well microtiter plate filled with LB medium. These "patients" can be infected with a mixture of bacteria, which may carry up to two resistance plasmids. Depending on the presence of bacteria and resistance, we assign each "patient" a resistance profile: uninfected (U), sensitive infected (S), single-resistant (A_r, B_r, or (A_r&B_r)), or double-resistant (AB_r).

In each experiment, we model six hospital wards to assess the ability of five treatment strategies (mixing, cycling, combination therapy with two antibiotics and two monotherapies with each antibiotic alone) and one control (no antibiotics) to contain the spread of plasmid-borne resistance and prevent the emergence of double resistance. All patients in each ward are treated daily according to the assigned strategy. A schematic of the experimental setup is shown in Figure S1. Each of the three experiments addresses a different scenario (Table 2.1), varying in patient turnover probability (admission/discharge), infection probability, and the distribution of resistance profiles for incoming patients (sampling proportions). The prevention scenario addresses a situation with low levels of pre-existing single and no double resistance brought into the hospital ward from the community. The containment scenario focuses on the ability of treatment strategies to contain pre-existing double resistance and in the maximum-emergence scenario, we maximised the opportunities for emerging double resistance through HGT by admitting single-resistant patients only.

Alongside our experiments, we created a computational model that mimics the experiment and is parameterised but not fitted using the experimental data. We used the model to assess the robustness of our findings to the randomisation of the experimental decisions and conducted an in silico sensitivity analysis to augment the experimental data.

2.3 Results

In each of our three experiments, we simulated the transition dynamics across six hospital wards on six 384-well plates. Each 384-well plate simulates four replicate hospital wards, with each replicate comprising 96 wells representing 94 patients and two negative controls. We replace each assay plate daily to renew the treatment and medium (Figure S1). Based on the turnover probability τ, we randomly decide if a patient stays. If this is the case, we inoculate the well on the new plate from the same well on the old plate. Else we replace this patient with a new incoming patient by inoculating the well on the new plate from a strain plate containing all resistance profiles. The resistance profile of the incoming patient is randomly selected based on predefined probabilities (sampling proportions c_ϕ). Based on the infection probability β, we randomly decide if a patient will infect another randomly chosen patient. These infections are then simulated in vitro by passing a drop to the infected well on the new plate. All inoculations are carried out using the same pintool.

Multidrug strategies keep the overall number of infections lowest and best suppress single resistance. The prevention scenario is characterised by a moderate proportion of single-resistant admissions to the hospital ward, the absence of pre-existing double resistance, and a moderately spreading infection dynamic ($R_0 = 1.5$, Equation S1, SI Methods). In this scenario, there are no differences between combination, mixing, and cycling on the frequency of uninfected, single-resistant-infected and double-resistant-infected wells (Fig. 2.1A, time series in Figure S2).

However, all multidrug strategies are significantly better at suppressing single resistance and increasing the number of cleared wells than the single-drug strategies and the control without treatment (Fig. 2.1A). In all scenarios, combination therapy was one of the most successful treatment strategies in minimising single-resistant and overall infections. At the same time, we

Table 2.1 Parameter sets and R_0 used in the three experiments: c_ϕ is the proportion of admitted patients with resistance profile ϕ, τ denotes the probability that a patient is replaced with a new patient sampled from the community and β denotes the infection probability.

scenario	c_S	c_{Ar}	c_{Br}	c_{ABr}	c_U	τ	β	R_0
prevention	0.75	0.05	0.05	0	0.15	0.20	0.30	1.5
containment	0.58	0.11	0.11	0.05	0.15	0.20	0.35	1.75
maximum-emergence	0	0.50	0.50	0	0	0.50	0.25	0.5

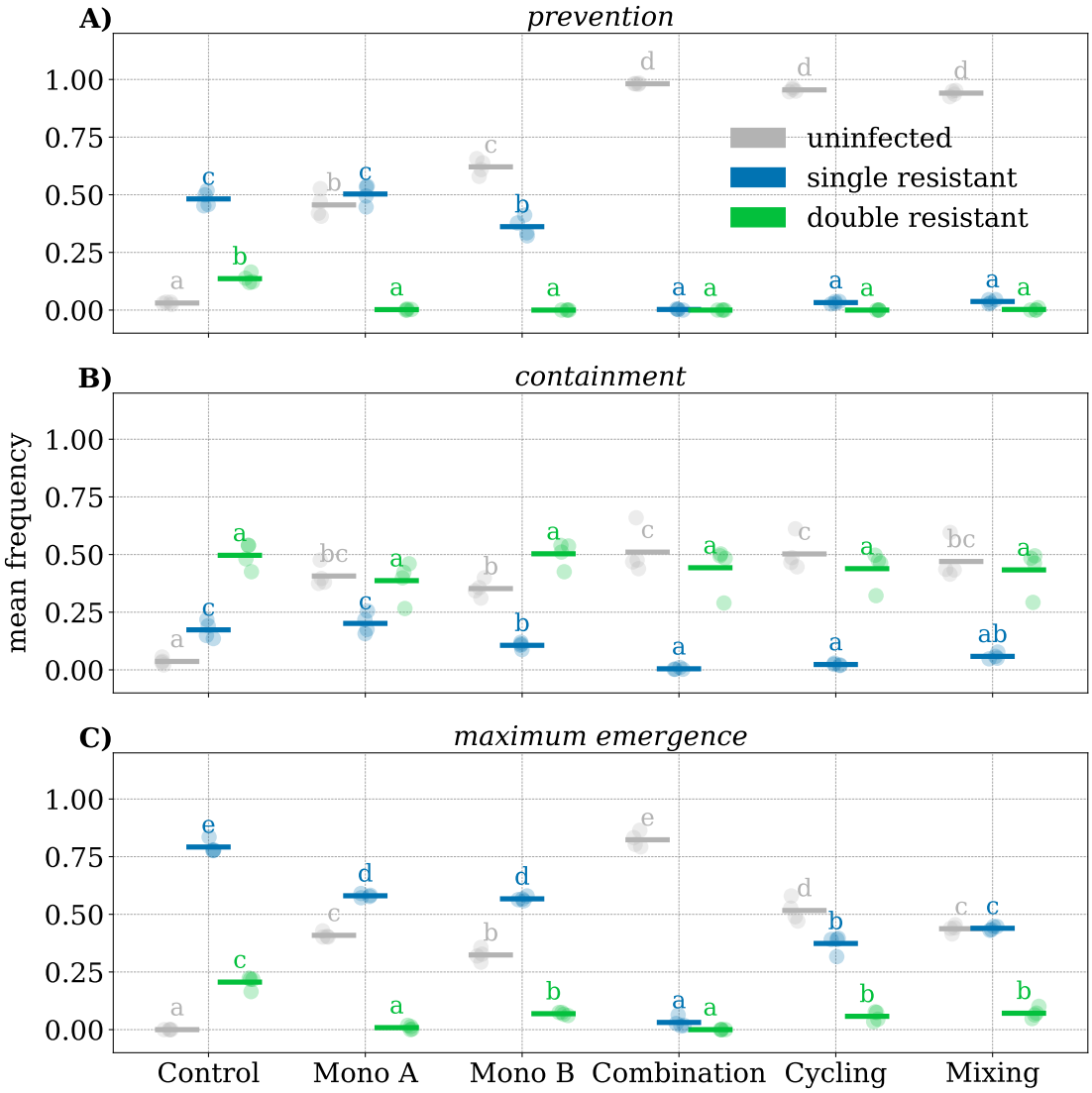

Fig. 2.1 Panels A–C show the mean frequency of uninfected (grey), single-resistant infected (blue), and double-resistant infected wells (green) during the last four transfers of the three scenarios. Circles represent replicates (n = 4), and bars represent means. Within resistance categories, bars not sharing a letter are significantly different (pairwise Tukey post hoc test, $p < 0.05$; ANOVA tables and all p-values can be found in Table S34 – S50).

observed most single and double resistance in the untreated control. All strategies (but not the control) were able to clear sensitive infections effectively with clearance probabilities of 97% for drug A, 73% for drug B, and 86% for AB (Table S8).

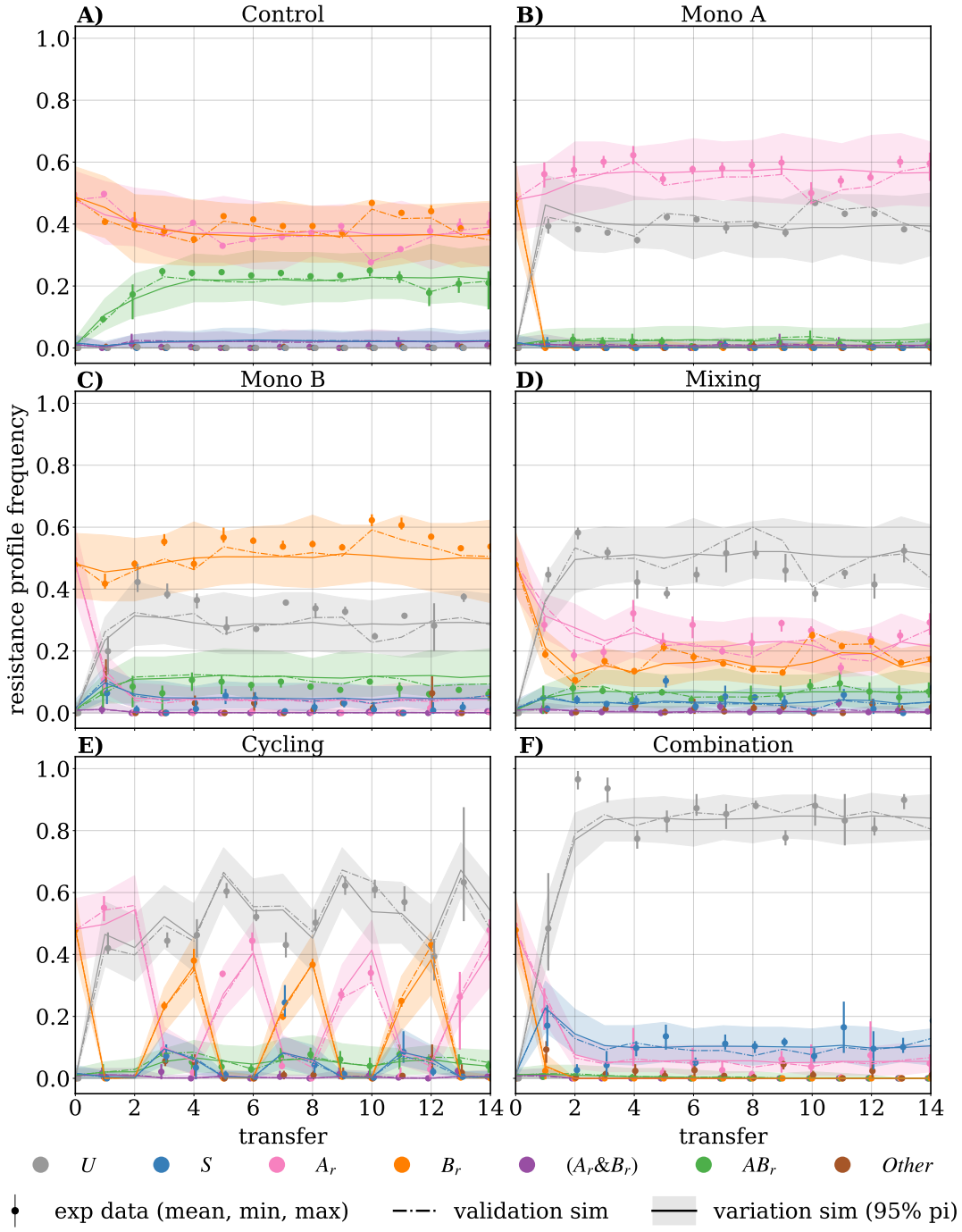

Fig. 2.2 Frequencies of resistance profiles over time during the maximum-emergence scenario. Panels (A–F) show the six tested strategies. Dots and bars show the mean and min/max interval of the four replicates. The dash-dotted line shows the mean value of 100 stochastic simulations based on the instruction set used in the in vitro experiment (validation simulation). The solid line shows the mean value of 100 simulations with randomly created instruction sets based on the parameter set used in the experiment (variation simulations). The shaded error band indicates the 95-percentile interval between the variation simulations.

All treatment strategies fail to contain pre-existing double resistance. The containment scenario explores a situation in which patients infected with double-resistant bacteria are continuously admitted to the hospital. No strategy was able to contain the spread of double resistance, resulting in increased frequencies of double resistance ($> 40\%$) in all treatment arms at the conclusion of the experiment (Fig. 2.1B).

Treatment strategies affect the emergence of double resistance. In our experiments, double resistance primarily emerges in wells inoculated with both single-resistance plasmids via HGT, as the evolution of de novo resistance (e.g. by point mutations) to high drug concentrations ($>$ 50×MIC) is unlikely. As the inoculum volumes for turnover, infection, and passage are identical in our experiments, we do not distinguish between wells containing A-resistance (A_r) infecting wells containing B-resistance (B_r) or vice versa and simply refer to these events as superinfections.

During the prevention and containment scenario, we could not identify differences in the strategies' abilities to suppress the emergence of double resistance. We attribute this to a lack of statistical power because we observed only a few instances of double resistance emerging, mostly in the untreated control. To address this, we selected parameters for the maximum-emergence scenario designed to maximise superinfection opportunities between wells carrying complementary resistance. To this end, all admitted patients carried bacteria with only one of the two resistance plasmids (at equal proportions). In addition, we set the probability of admission and discharge to $\tau = 0.5$ and the infection probability to $\beta = 0.25$, resulting in a basic reproduction number $R_0 = 0.5$ (Equation S1). An $R_0 < 1$ makes double resistance more likely to be replaced by newly admitted patients than to spread, thus maintaining a high potential for emergence. We implement this scenario to explore emergence under a magnifying glass, being aware that it does not reflect a likely clinical situation. In this scenario, combination therapy and monotherapy with drug A lead to the lowest frequency of double resistance during the last four transfers (Fig. 2.1C, Fig. 2.2).

For the maximum-emergence scenario, we observed that combination therapy, cycling, and monotherapy with drug A were most effective in preventing newly emerging double resistance. Combination was the only strategy in which we did not observe a single case of emerging double resistance after the first transfer (Fig. 2.3A). Furthermore, combination therapy is the most successful treatment strategy in minimising the number of both single-resistant and overall infec-

tions, while the control leads to the highest number of double- and single-resistant, and overall infections.

Combination therapy suppresses the emergence of double resistance by preventing superinfections. Treatment strategies can impact the emergence of double resistance by suppressing superinfections. The number of superinfections $n_{\mathscr{S}}$is dependent on the abundance of the single resistance carrying wells A_r and B_r. Hence, we expect the highest number of superinfections and most opportunities for emerging double resistance when both single resistances are unaffected by the treatment and the fewest if the treatment successfully suppresses both single resistances. Our measurements confirmed these expectations during the maximum-emergence scenario. Here $n_{\mathscr{S}}$is highest in the control group (no treatment) and lowest under combination therapy (Fig. 2.3B).

Treatment strategies influence the emergence of double resistance within superinfected wells. We observed the highest average frequency of superinfections developing double resistance ($\frac{n_{\mathscr{E}}}{n_{\mathscr{S}}}$) in antibiotic-free medium and in medium treated with antibiotic B (tetracycline). In contrast, superinfections resulting in double resistance rarely occur in medium treated with antibiotic A (ceftazidime) or both drugs (Fig. 2.3C). We think the impact of treatment on cell densities within superinfected wells (both in infected and infecting wells) can best explain these findings.

Firstly, applying a drug affects the in-well population dynamics of superinfected wells. Reducing the cell density for one or both single-resistant strains within a superinfected well reduces the probability of bacteria with complementary resistance to encounter and conjugate (see SI Results). As drug A (bactericidal) decreases the cell density faster than drug B (bacteriostatic), more conjugation opportunities occur in wells treated with drug B.

Secondly, the treatment strategies influence the number of transferred single-resistant bacteria that inoculate superinfections by curbing the bacterial density within the infecting wells (see SI Results).

Due to the differences in the abilities of drugs A and B to prevent conjugation, there are times (cycles) and places (beds) during cycling and mixing where using drug B offers increased opportunities for the emergence of double resistance, which is never the case with combination therapy.

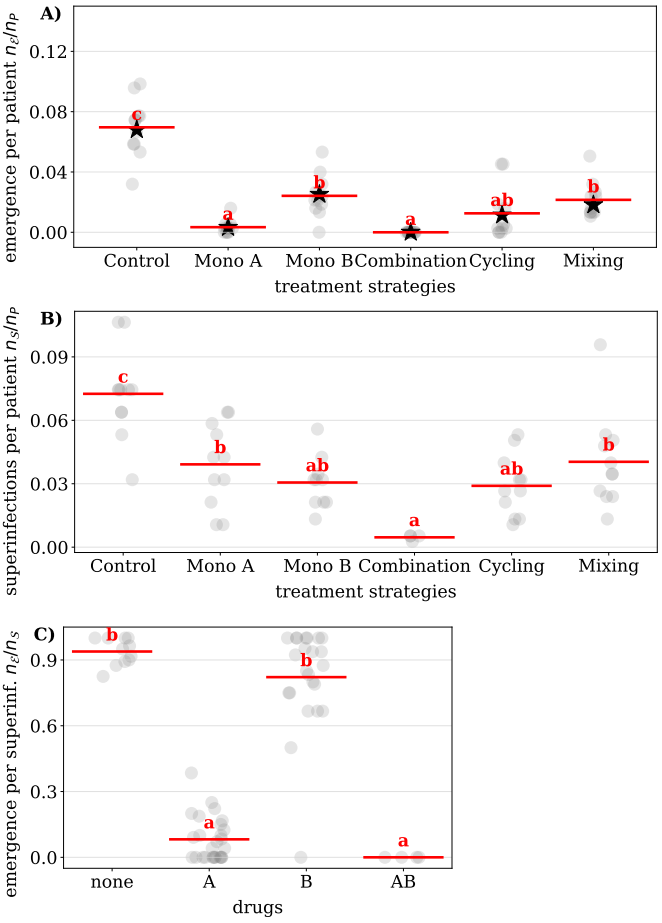

Fig. 2.3 Analysis of the emergence of double resistance in vitro and superinfection between single resistant A_r and B_r wells during the maximum-emergence scenario, from transfer four onwards. Each dot corresponds to data from a single plate, with each plate representing a distinct treatment arm, encompassing 376 patients for one transfer. Mean values are represented by red bars. Bars not sharing a letter are significantly different ($p < 0.05$, ANOVA tables and pairwise Tukey post hoc results can be found in Table S51 – S56). A) Number of newly emerged cases of double resistance per plate ($n_\mathscr{E}$), normalised to the total number of patients (n_P = 376). B) Number of superinfections per plate ($n_\mathscr{S}$), normalised to n_P. C) Proportion of superinfected wells treated with A, B, AB, or none that develop double resistance.

Computational model corroborates the robustness of experimental outcomes. The experiments are conducted by a liquid handling platform that carries out predefined instructions, specifying which infections occur and who is admitted or discharged. The instructions are randomized based on parameter sets we defined for each scenario, including the overall infection and turnover probability as well as the distribution of the resistance profiles of admitted patients. We call the entirety of all instructions that come up during one experiment an 'instruction set'. Due to the scale and technical complexity of the experiments, it was not feasible to carry out individual instruction sets for each replicate, so we opted to apply the same instruction sets for all replicates. This raises the question of whether the experimental results are a consequence of a specific instance of this random process and whether they are robust to the randomisation in the instruction set. To address this, we developed a discrete-time stochastic model comprising

94 individual in silico patients mimicking the epidemiological dynamics of the experiment (SI Computational Model). The model was parametrised, but not fitted, with transition probabilities (Table S18–S25) that we estimated based on the transition frequencies measured in vitro. We used the same transition probabilities in the simulations for all scenarios.

First, we validated the model by averaging 100 validation simulations, each employing the identical instruction sets used in vitro. The aim of the validation simulations is to recreate the experiments in silico (Figure S3B). We found that the simulation results are in good agreement with the experimental data, indicating that the model reflects the dynamics observed in the in vitro experiments well (see Fig. 2.2, Figure S2, and Figure S4). One exception is the spread of A-resistance during the prevention scenario in control and Mono A. This could indicate an increased number of contaminations at the beginning of the prevention scenario. We also observe some discrepancies for the spread of double resistance during the prevention scenario, which we attribute to contamination artefacts in the transition probabilities (see SI Computational Model).

Second, we averaged 100 variation simulations to assess the robustness of the experimental outcomes against variations in the instruction sets. In these variation simulations, each of the 100 instruction sets was randomized based on the same three parameter sets used in vitro (Figure S3C). Differences between the validation and variation simulations indicate differences in outcome due to the randomization of the instruction sets. For instance, with a turnover probability $\tau = 0.2$ and an admission probability $c_A = 0.05$, we expect $0.94\ A_r$ admissions per transfer. However, random fluctuations can result in either more (or fewer) A_r admissions, leading to a temporarily higher (or lower) frequency of A_r in the validation simulations, creating a temporary spread between the validation and variation simulations. We observed that the validation simulations fluctuate around the variation simulations and never diverge far (see Fig. 2.2, Figure S2, and Figure S4), indicating robustness of the experimental results to the randomisation of the instruction sets.

***In silico* sensitivity analysis indicates that the superiority of combination therapy is robust.** Given that the validation simulations agreed well with the experiments, we used the model to perform an in silico parameter sensitivity analysis of the experimental results (Figure S3D). To this end, we ran ten simulations for each of 20,000 randomly generated parameter sets by varying the

turnover and infection probability and the five sampling proportions for incoming patients: (τ, β, c_S, c_{A_r}, c_{B_r}, c_{AB_r}, c_U). For half of the parameter sets, we forced the frequency of incoming patients with double resistance (c_{AB_r}) to zero.

We used the frequency of uninfected in silico patients to measure treatment success. Using this criterion, the control strategy (no treatment) always performed worst, and accordingly, we excluded this treatment arm from the following analysis. Strategies were then classified as (i) 'single winners' if they are significantly better than all other strategies; (ii) 'winners' if they are not outperformed by any other strategy; (iii) 'losers' if they do not outperform at least one other strategy; or (iv) 'single losers' if all other strategies outperform them.

In parameter sets with and without pre-existing double resistance, combination therapy ranks most often as one of the best strategies (87% and 98%, respectively). It is the single best strategy in 55% of the tested parameter sets with pre-existing double resistance and in 93% of cases without pre-existing double resistance (Fig. 2.4, Table S14, Table S15).

In some situations (for example, when one strategy is much worse than all others), it is more important to avoid the worst strategy than selecting the very best strategy among the good ones. Our analysis finds that combination therapy is almost never among the worst strategies, while usually one of the two monotherapies performs worst. As expected, single-drug strategies perform particularly poorly when there is a high frequency of pre-existing single-resistance to the applied drug (Table S11, Table S13).

Cycling and mixing lose substantially less than the monotherapies but are rarely the single best strategy.

2.4 Discussion

In our study, multi-drug strategies, particularly combination therapy, outperformed monotherapies in reducing overall infections and the emergence of double resistance across most scenarios, while we observed most emergence of double resistance in the untreated control. Interestingly, the effectiveness of combination therapy does not stem from an increased efficacy associated with higher doses. This is because an asymmetrical antagonism exists between the bactericidal antibiotic ceftazidime (drug A) and the bacteriostatic antibiotic tetracycline (drug B), resulting in a lower clearance rate for the combination A+B compared to drug A alone (SI Results). This

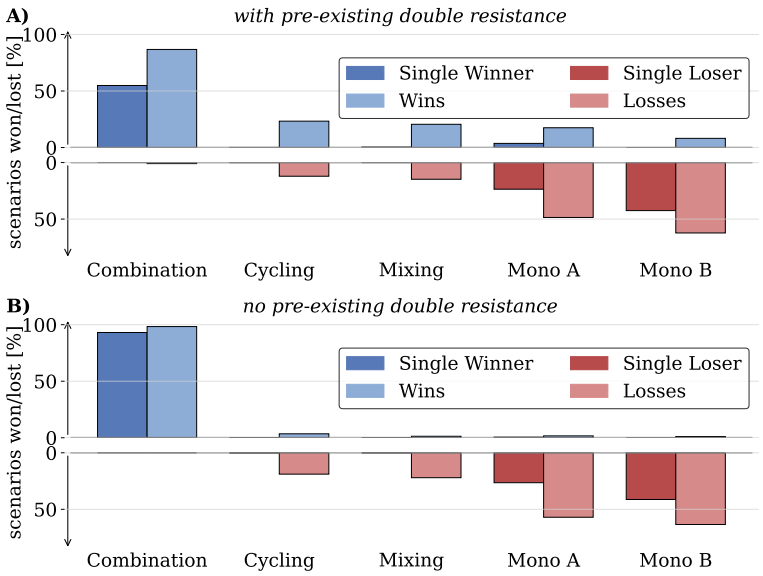

Fig. 2.4 Effectiveness of the five treatment strategies in maximising the frequency of uninfected individuals across randomly generated parameter sets. Strategies not significantly better than any other are marked as losers (pastel red), and those significantly worse than all others as single losers (dark red). Strategies not significantly worse than any other are classified as winners (pastel blue), and those significantly better than all others as single winners (dark blue). Strategies without significant differences were excluded. (A) 10,000 parameter sets with pre-existing double resistance. 606/10,000 sets yielded no significant difference between the strategies. (B) 10,000 parameter sets without pre-existing double resistance. 100/10,000 sets yielded no significant difference between the strategies.

observation implies that combination therapy may be even more advantageous when drugs are neutral or synergistic towards each other.

Why does the absence of treatment lead to worse outcomes, and why is combination therapy preventing the emergence of double resistance so effectively?

First, we measured the presence, not the density, of resistant bacteria in wells by assessing if small aliquots of the liquid culture could grow on treated agar plates. This approach quantifies the number of wells hosting a specific resistance but can not quantify the frequency of resistance in the in-well population. The information about presence/absence alone yields important information about potential treatment success and is used in analogous clinical diagnostic methods, such as disk diffusion tests [13].

We would only recognize a loss of resistance (in the experiments and clinical samples) if the

resistant strain were fully outcompeted. This was not observed during the containment scenario in the untreated control. Such an outcome was expected due to the short average patient stay of 2–5 days in our experiments and 5–6 days in clinical situations [14]. For the same reason, we would not expect an eradication of resistance but only a shift in resistance density, even if there were more substantial costs of resistance or higher segregational loss. In our experiments, we found no evidence of a cost of resistance (see SI Methods, Figure S6, and Table S3) or segregational loss (see SI Methods and Table S4).

Second, in our experiments, the emergence of double resistance requires conjugation, which relies on superinfection between hosts with complementary resistance profiles. As demonstrated in Fig. 2.3B, the lowest number of superinfections occur in combination therapy, where both single-resistant strains can be cleared. Conversely, without treatment, the abundance of single resistance is highest resulting in the highest number of superinfections.

Third, the applied antibiotics affect the frequency of superinfections leading to double resistance, likely by influencing the growth dynamics within the superinfected well and potentially the conjugation rate [15]. However, our experimental data are unsuitable for supporting or rejecting the impact on conjugation rates. We observed the least emergence of double resistance in superinfected wells treated with both drugs and most in untreated wells, contributing to the superiority of combination therapy and the high rates of double resistance in the absence of treatment (Fig. 2.3C). This effect on the in-well dynamics may be a property of the chosen drugs and concentrations, and we expect better results for cycling and mixing if both drugs were equally effective in suppressing double resistance or worse results for combination therapy if the combination of both drugs was less effective.

Fourth, we observed that the number of single-resistant bacteria inoculating superinfections impacts the frequency of emerging double resistance (see SI Results, Table S1). In our setup, superinfected wells receive two inocula, with at least one inoculum transferred from the previous plate (by infection) that has already undergone treatment for one day. When prior treatment led to a low bacterial density in the source wells, we did not observe any cases of double resistance emerging. This could magnify the effectiveness of combination therapy, where all potential single-resistant inocula transferred from the previous plate contain low bacterial densities due to effective treatment. On the one hand, this may be more a characteristic of our experimental

setup due to the fixed length of the treatment interval and high clearance probabilities. On the other hand, we indeed expect fewer cases of emergence in superinfected patients if the infecting inocula are small.

In our experiments and simulations, combination therapy showed superior results in minimizing infections and preventing double resistance. This advantage may partly result from assumptions and simplifications, including the chosen strain, drugs, plasmids, and inoculum size, the discrete setup with fixed treatment durations, colonization-independent infection and turnover probabilities, and the absence of an immune system and microbiome. Also, treating all patients irrespective of colonization diverges from clinical reality in two ways: i) in a clinical setting, some untreated patients may serve as a sanctuary for resistance and a potential source of double resistance and ii) treating all patients, regardless of infection status, contrasts with clinical efforts to promote targeted antibiotic use. However, since patients as we model them in our in vitro experiments lack a microbiome, treating uninfecteds should have no impact on the resistance dynamics.

Despite the numerous differences between our experiments and a real clinical situation, we argue that the relative effectiveness of combination therapy in suppressing double resistance would likely translate to real patients. The reason is that the emergence of double resistance hinges on two critical processes: 1) preventing superinfections between patients carrying bacteria with complementary resistance plasmids and 2) the probability that superinfected hosts develop double resistance. We think that combination therapy offers a strategic advantage in addressing both processes.

Our results complement the findings by Angst et al. [10], who observed similar outcomes in the context of chromosomal resistance. We believe that such in vitro experimental models, which explore admittedly idealised and simplified epidemiological scenarios, can help to bridge the divide between mathematical models and randomised clinical trials. However, ultimately the evidence for or against the benefits of combination therapy must be confirmed by rigorous clinical trials with sufficient statistical power to support or challenge the effectiveness of combination therapy.

2.5 Methods

Drugs and Media. In all experiments, we used LB (Sigma L3022) with 25 $\mu g/ml$ (prevention scenario) or 5 $\mu g/ml$ (containment and max-emergence scenario) chloramphenicol as a liquid medium and the same LB and drugs with 1.5% agar as a solid medium. Chloramphenicol was added to prevent external contaminations. We could not measure any significant growth effects of the chloramphenicol concentrations on the chloramphenicol-resistant strains (see Table S5). We used 80 $\mu g/ml$ ceftazidime as drug A and 40 $\mu g/ml$ tetracycline as drug B, with identical concentrations for liquid and solid media.

Strains and Plasmids. We used two compatible plasmids p_A and p_B derived from samples ESBL9 and ESBL25 from a clinical transmission study [12]. Samples were kindly provided by Adrian Egli and sequenced and analysed by Huisman et al. [11]. Plasmids p_A and p_B provide (among other resistances) resistance against drug A and drug B, respectively. We used these plasmids and the chloramphenicol-resistant host MDS42-YFP [16] (sensitive to drugs A and B) to create three additional strains by conjugation (Table S2) (i) A-resistant, containing p_A; (ii) B-resistant, containing p_B; and (iii) AB-resistant, containing both plasmids (see SI Methods).

Treatment arms. We simulated the epidemiological dynamics of six hospital wards in vitro, with each ward exploring a different treatment arm: (i) control with no treatment, (ii) monotherapy with ceftazidime (mono A), (iii) monotherapy with tetracycline (mono B), (iv) cycling therapy (A, A, B, B, ...), (v) mixing therapy (treatment A and B are randomly assigned daily, without knowledge of prior treatment), and (vi) combination therapy (treating all patients with both drugs, each at full concentration).

Assay plates. Each hospital ward was simulated in vitro on a 384-well microtiter plate (Greiner 781186). Wells are interpreted as beds in four replicate hospital wards with 94 beds each. The remaining wells contained only growth medium and remained untouched, acting as sentinels for contamination. Across all experiments and treatment arms, 2752 control wells were used, 67 of which became contaminated. Wells with growth medium but no bacteria represent uninfected patients, whereas wells with growth medium and (resistant or sensitive) bacteria represent infected patients.

Experimental procedure. Experiments were performed using a Tecan Evo 200 automated liquid handling system (Tecan) with an integrated, automated incubator (Liconic STX100, Liconic), a Tecan Infinite F200 spectrophotometer (Tecan), and a camera (Pickolo, SciRobotics).

Every day new assay plates were filled with 45 µl fresh medium and 5 µl antibiotic stock, according to its designated treatment strategy (see Figure S1). At each of these transfers, we simulate patients staying overnight in the hospital (passage), the admission and discharge of patients (turnover), and infections between patients (infection). Passage, turnover and infections were all done by inoculating the new plate using a pintool with retractable pins, as detailed below, carrying ≈0.3 µl drops between wells ($\approx 1:150$ dilution) leading to an approximately 6-8 hours exponential phase. The assay plates were then incubated at 37 °C and 95% relative humidity. The incubation duration varied due to variations in the time it takes to set up a new transfer and occasional transfer repetitions made necessary because of machine errors or user mistakes. The mean incubation duration was 27 hours.

We initiated the experiment by inoculating one 384-well plate from fresh overnight cultures representing patients from an outside community. We assume that this community is sufficiently large to be unaffected by interactions with the hospital ward. Incoming patients are either uninfected or carry one of the four strains (sensitive, each single resistant or double resistant) and are sampled according to predefined sampling proportions, defining the probability of a resistance profile being admitted to the hospital. (Table 2.1). This initial plate remained untreated and was used as the initial population for all six treatment arms.

Turnover. Every transfer, each patient has a turnover probability τ to be discharged from the hospital and replaced by a newly admitted patient. Wells representing staying patients were passed from the previous to the new assay plate using the pintool. Here, the pins for discharged patients are retracted. Vacant beds on the assay plate were then reoccupied by patients from the community analogous to the initial setup.

Infections. To simulate infections, each well has an infection probability β to infect another randomly chosen well on the next assay plate during the transfer. Therefore, each patient can infect at most one other patient per transfer, but several patients could potentially infect the same patient.

Resistance Profiles. To assess the resistance profile of each well, we spotted the previous assay plate onto four agar plates, using the pintool. Three plates were treated with antibiotics (A, B, or AB), while one was untreated (none). After incubation at 37 °C and 95% relative humidity, images of the agar plates are taken and analysed using the Pickolo package (SciRobotics, Kfar Saba, Israel). The software automatically detects the presence of colonies at each well position, which we also manually verified. The growth pattern on the four agar plates allowed us to determine the resistance profile of a well, which reflects how the well would behave if treated.

By default, we distinguish six resistance profiles (Table S6). The wells may either be 1) uninfected (U), 2) exclusively infected with sensitive bacteria (S), 3) infected with A-resistant bacteria (A_r), 4) infected with B-resistant bacteria (B_r), 5) infected with AB-resistant bacteria (AB_r), 6) or be infected with a mixed population containing A-resistant and B-resistant bacteria, but no AB-resistant bacteria ($(A\&B)_r$). The way we classify the resistance profiles of the bacterial population in a well leads to the dominance of resistance, in the sense that a predominantly sensitive population harbouring a resistant minority would be classified as resistant (see Table S7). Any observed growth pattern not corresponding to the six resistance profiles mentioned above is classified as 'other'. The resistance profile 'other' primarily occurs when bacterial densities are low (see also SI Methods).

Scenarios. We conducted experiments for three scenarios (prevention, containment, and maximum-emergence) with 14 to 27 transfers each. Each experiment was defined by a different parameter set consisting of (i) the infection probability β within the hospital, (ii) the turnover probability τ and (iii) the sampling proportions c_ϕ of patients with resistance profile $\phi \in \{U, S, A_r, B_r, AB_r\}$ (see Table 2.1).

The prevention scenario (Figure S2) addresses how the treatment strategies perform with a moderately resistant community and a moderate infection regime in the hospital ward and how well they are able to prevent the upcoming double resistance.

The containment scenario (Figure S4) corresponds to a scenario in which some patients entering the hospital are infected with double-resistant bacteria to compare the ability of treatment strategies to contain the spread of pre-existing double resistance.

During the maximum-emergence scenario (Fig. 2.2) 50 % of the incoming patients are infected

with A-resistant bacteria, and the other 50 % are infected with B-resistant bacteria. These conditions maximally favour opportunities for horizontal gene transfer. The basic reproduction number was set to $R_0 = 0.5$ (Equation S1) to ensure that double-resistant strains are flushed out, reducing the stochastic dependency on earlier emergence events while maintaining a high potential for new emergence.

Instruction Sets. Based on the parameter defined for each experiment (see Table 2.1), we generated instructions that were passed to the liquid handling platform. These instructions specify which patients are passaged or discharged and admitted, who infects whom, and the treatment for mixing therapy. Instructions are randomly generated prior to each transfer. We call the entirety of all instructions that come up during an experimental run an instruction set. Instruction sets are identical across all treatment arms and replicates.

Computational Model. We created a stochastic model (SI Computational Model) incorporating 94 in silico patients, each capable of adopting one of six resistance profiles $\phi \in \{U, S, A_r, B_r, AB_r, (A_r \& B_r)\}$. The model is structured analogue to the in vitro experiments (Figure S1) and alternates between modelling the transactions between wells and the effect of treatment during incubation.

Admission and discharge (turnover) were simulated by replacing the resistance profile of the current patient with that of the incoming patient, as defined by the instruction set. Infections are simulated by combining the resistance profiles of the receiving well i and the infecting well j. The resulting resistance profile $\phi_i + \phi_j$ is determined using the rules based on the dominance of resistance specified in Table S9. Calculations involving more than two resistance profiles apply the associative law and are determined pairwise, e.g. $(U + S) + A_r = S + A_r = A_r$.

To model treatment effects, we use transition probabilities to assign the post-incubation resistance profile $\phi(\hat{T})$ stochastically based on the treatment and the pre-incubation resistance profile $\phi(T)$. The transition probabilities (Table S18 – S25) were estimated based on experimental data across all experiments.

***In Silico* Sensitivity Analysis.** To augment the experimental data, we conducted an in silico sensitivity analysis. We randomly generated 10,000 parameter sets with and 10,000 without pre-existing double resistance. Turnover and infection probabilities were uniformly sampled

$[0.05, 0.95]$, allowing for $R_0 \in [0.0526, 19]$. The sampling proportions c_ϕ for all incoming resistance profiles ($\phi \in \{U, S, A_r, B_r, AB_r\}$) were randomised by sampling a number $n_\phi \in [0, 1]$ from a uniform distribution and subsequently normalising by the sum: $c_\phi = n_\phi / \sum_j n_j$. We created ten randomised instruction sets for each parameter set and conducted one simulation per instruction set (Figure S3D) for 28 transfers.

For this analysis, the frequency of non-infected individuals during the last four transfers was used as a performance metric for treatment strategies, as it also indirectly reflects the frequency of both double- and single-resistant patients. We conducted an ANOVA test to assess if the effect of the treatment strategies significantly ($p < 0.05$) influences the frequency of uninfecteds. For significant tests, we proceeded with Tukey's post hoc analysis ($p < 0.05$), identifying significantly distinct pairs of strategies. Strategies not significantly inferior to others were classified as 'winners', while strategies not significantly superior to any were classified as 'losers'. Strategies that win or lose a parameter set alone are 'single winners' or 'single losers'.

Data Availability Experimental data and analysis scripts, as well as code for the computational model, have been deposited in Zenodo (`https://doi.org/10.5281/zenodo.14137410`).

Acknowledgments

We thank Adrian Egli for generously providing the ESBL samples containing the plasmids and Fabienne Benz and Jana Huisman for their assistance with selecting them. We also thank Lukas Graz from the Seminar for Statistics (ETHZ) for his statistical consultation. We used Grammarly and OpenAI's ChatGPT for proofreading and grammar checking. We thank ETH Zurich for providing funding.

Bibliography

[1] .P. F. Kable and H. Jeffery. "Selection for Tolerance in Organisms Exposed to Sprays of Biocide Mixtures: A Theoretical Model". In: Phytopathology 70.1 (1980), pp. 8–12. issn: 0031-949X. doi: 10.1094/phyto-70-8.

[2] .C. J. Delp. "Coping with resistance to plant disease". In: Plant Dis. 64 (1980), pp. 652–657. doi: 10.1094/PD-64-652.

[3] .G. Skylakakis. "Effects of Alternating and Mixing Pesticides on the Buildup of Fungal Resistance". In: Phytopathology 71.11 (1981), pp. 1119–1121. issn: 0031-949X. doi: 10.1094/phyto-71-1119.

[4] .D. E. Goldberg, R. F. Siliciano, and W. R. Jacobs. "Outwitting evolution: Fighting drug-resistant TB, Malaria, and HIV". In: Cell 148.6 (2012), pp. 1271–1283. issn: 10974172. doi: 10.1016/j.cell.2012.02.021.

[5] .B. Siedentop, V. N. Kachalov, C. Witzany, M. Egger, D. Roger, and S. Bonhoeffer. "The effect of combining antibiotics on resistance : A systematic review and meta-analysis". In: Elife 13 (2024), pp. 1–25. doi: 10.7554/eLife.93740.1.

[6] .P. J. van Duijn et al. "The effects of antibiotic cycling and mixing on antibiotic resistance in intensive care units: a cluster-randomised crossover trial". In: Lancet Infect. Dis. 18.4 (2018), pp. 401–409. issn: 14744457. doi: 10.1016/S1473-3099(18)30056-2.

[7] .H. Uecker and S. Bonhoeffer. "Antibiotic treatment protocols revisited: The challenges of a conclusive assessment by mathematical modelling". In: J. R. Soc. Interface 18.181 (2021). issn: 17425662. doi: 10.1098/rsif.2021.0308.

[8] .S. Bonhoeffer, M. Lipsitch, and B. R. Levin. "Evaluating treatment protocols to prevent antibiotic resistance". In: Proc. Natl. Acad. Sci. U. S. A. 94.22 (1997), pp. 12106–12111. issn: 00278424. doi: 10.1073/pnas.94.22.12106.

[9] .B. Tepekule, H. Uecker, I. Derungs, A. Frenoy, and S. Bonhoeffer. "Modeling antibiotic treatment in hospitals: A systematic approach shows benefits of combination therapy over cycling, mixing, and mono-drug therapies". In: PLoS Comput. Biol. 13.9 (2017), pp. 1–22. issn: 15537358. doi: 10.1371/journal.pcbi.1005745.

[10] .D. C. Angst, B. Tepekule, L. Sun, B. Bogos, and S. Bonhoeffer. "Comparing treatment strategies to reduce antibiotic resistance in an in vitro epidemiological setting". In: Proc. Natl. Acad. Sci. U. S. A. 118.13 (2021), pp. 1–7. issn: 10916490. doi: 10.1073/PNAS.2023467118.

[11] .J. S. Huisman, T. G. Vaughan, A. Egli, S. Tschudin-Sutter, T. Stadler, and S. Bonhoeffer. "The effect of sequencing and assembly on the inference of horizontal gene transfer on chromosomal and plasmid phylogenies". In: Philos. Trans. R. Soc. B Biol. Sci. 377.1861 (2022). issn: 14712970. doi: 10.1098/rstb.2021.0245.

[12] .S. Tschudin-Sutter, R. Frei, F. Schwahn, M. Tomic, M. Conzelmann, A. Stranden, and A. F. Widmer. "Prospective validation of cessation of contact precautions for extended-spectrum β-lactamase-producing Escherichia coli1". In: Emerg. Infect. Dis. 22.6 (2016), pp. 1094–1097. issn: 10806059. doi: 10.3201/eid2206.150554.

[13] .European Committee on Antimicrobial Susceptibility Testing (EUCAST). Antimicrobial susceptibility testing EUCAST disk diffusion method Version 12.0 January. 2024.

[14] .K. Hofstetter, E. Salgado-Thalmann, and M. Bachmann. Kennzahlen der Schweizer Spitäler 2015. 2017.

[15] .B. Headd and S. A. Bradford. "Physicochemical factors that favor conjugation of an antibiotic resistant plasmid in non-growing bacterial cultures in the absence and presence of antibiotics". In: Front. Microbiol. 9 (2018), pp. 1–14. issn: 1664302X. doi: 10.3389/fmicb.2018.02122.

[16] .T. Fehér, B. Bogos, O. Méhi, G. Fekete, B. Csörg, K. Kovács, G. Pósfai, B. Papp, L. D. Hurst, and C. Pál. "Competition between transposable elements and mutator genes in bacteria". In: Mol. Biol. Evol. 29 (2012), pp. 3153–3159. issn: 0737-4038. doi: 10.1093/molbev/mss122.

2.6 Supplementary Information

SI Methods

Strains We chose two plasmid-carrying donors, ESBL9 and ESBL25, and two drugs, ceftazidime and tetracycline, based on the resistance conferred by the plasmids contained in the strains and the compatibility of the plasmids. ESBL9 and ESBL25 were collected as part of a clinical transmission study at the University Hospital Basel, Switzerland [1] and fully sequenced, including identification of the carried plasmids [2]. The strains were a generous gift from Adrian Egli, University Hospital Basel.

ESBL9 contains an IncI1 plasmid, referred to here as p_A, conferring, among others, resistance to ampicillin and ceftazidime but not tetracycline or chloramphenicol. ESBL25 contains an IncF1 plasmid, referred to here as p_B, conferring, among others, resistance to ampicillin and tetracycline but not ceftazidime or chloramphenicol.

The two plasmids were transferred by conjugation from the original clinical isolates to the chloramphenicol-resistant and ampicillin-sensitive Escherichia coli MDS42-YFP (recipient) [3], followed by selection for ampicillin and chloramphenicol resistance. This results in the ceftazidime-resistant (A-resistant) strain and the tetracycline-resistant (B-resistant) strain. The double-resistant (AB-resistant) strain was created by a further round of conjugation to receive both plasmids and subsequent selection for ceftazidime and tetracycline resistance. Strains are listed in Table 2.3. All transconjugants were verified by PCR replicon typing using primers specific for the respective replicon [4].

Drugs. We used ceftazidime, referred to as drug A, at a concentration of $80\,\mu g\,mL^{-1}$. $80\,\mu g\,mL^{-1}$ is substantially lower than the MIC for A-resistant bacteria and more than 50 times the MIC for sensitive or B-resistant bacteria. Using the same reasoning, we used tetracycline, referred to as drug B, at a concentration $40\,\mu g\,mL^{-1}$. The antibiotic concentrations in the liquid and the solid media were identical. To avoid contamination, we used $25\,\mu g\,mL^{-1}$ chloramphenicol for prevention scenario and $5\,\mu g\,mL^{-1}$ chloramphenicol for containment and maximum-emergence scenarios. We could not measure any significant growth effects of the chloramphenicol concentrations on the chloramphenicol-resistant strains (see Table 2.6).

Conjugation Protocol. We used ampicillin-resistant and chloramphenicol-sensitive original donors [1, 5] and the chloramphenicol-resistant, ampicillin-sensitive recipient [3]. Fresh overnight cultures of both donors and recipients were diluted 1:1000 and grown to mid-exponential phase. Following this, the donor and recipient cultures were combined in a culture tube and incubated for four hours at 37 °C with constant shaking at 180 rpm. We then spotted a 100 µl drop of this mixture on an agar plate treated with $25\,\mu g\,ml^{-1}$ chloramphenicol and $100\,\mu g\,ml^{-1}$ ampicillin, allowing only the transconjugants to grow. Conjugation was verified by PCR replicon typing [4].

Plasmid costs To measure plasmid costs, we grew three replicates of overnight cultures of all strains in selective medium. The cultures were then diluted approximately 1:150 into LB with 5 $\mu g/ml$ chloramphenicol using the pintool, following the same procedure as in the main experiments. Subsequently, we recorded OD growth curves using the same plate reader. The maximum growth rate was estimated by applying linear regression to a sliding window on the log-transformed data (window size: 1 hour, step size: approximately 5 minutes). Pairwise comparisons were performed between the maximum growth rates of the sensitive strain and the plasmid-carrying strains using the Mann-Whitney U test (scipy.stats [6]), followed by a Bonferroni correction to account for multiple testing. We observed no significant difference in the maximum growth rate between any of the pairs (Table 2.4).

Segregational Loss We estimated plasmid segregation loss over 24 hours (t_0–t_1) without treatment and with treatment as a control. For this, we grew overnight cultures in selective medium for three replicates $k \in \{1,2,3\}$ of each plasmid-carrying strain. We diluted the cultures and plated each on drug-free agar plates, followed by replica plating onto selective plates to identify the presence or absence of resistance plasmids in each colony. This initial step represents time point t_0. The overnight cultures were then transferred to i) drug-free medium and ii) selective medium (control), using the same pintool as in the main experiments. The cultures were incubated for 24 hours, after which we diluted and plated them again on drug-free plates and used replica plating on selective plates to assess plasmid presence for time point t_1. We compared the frequencies $f_k(t)$ of plasmid presence between time points t_0 and t_1 using the Mann-Whitney U test (scipy.stats [6]). No significant loss of plasmids was observed in either the control or the experimental conditions (Table 2.5). We estimated the mean frequency of plasmid presence $f(t)$ for

each strain and time point and the confidence intervals $CI(t)$ for the frequency by bootstrapping the pooled colony presence-absence data.

Growth rates and bacterial density. We assessed the final bacterial density of overnight cultures following an 18-hour incubation period (Table 2.6) for each bacterial strain in its respective selective medium for two different chloramphenicol concentrations: $5\,\mu g\,mL^{-1}$ and $25\,\mu g\,mL^{-1}$. To estimate the bacterial density, we plated $200\,\mu L$ of various dilutions of the cultures on agar plates using glass beads. The 95 % confidence intervals for the colony counts were calculated using the Poisson distribution.

In addition, we monitored the optical density (OD) in 384-well plates over an 18-hour period in the respective selective medium containing either $5\,\mu g\,mL^{-1}$ or $25\,\mu g\,mL^{-1}$ chloramphenicol. To determine the maximum growth rates, we employed a sliding window approach with a one-hour width, linearly fitting the growth rate to the log transformed values within this window for each replicate. The 95 % confidence intervals for the maximal growth rates were calculated using the Student's t-distribution.

Basic Reproductive Number. R_0 represents the number of secondary infections generated by one patient in a fully susceptible population. Let τ denote the probability that a patient leaves the hospital ward after one timestep, $\tau' = 1 - \tau$ the probability that the patient stays and β the probability that a patient infects another during one timestep. Then we can write the total number of infections caused by one patient introduced into a susceptible population as a geometric series:

$$R_0 = (\tau')^0 \cdot \beta + (\tau')^1 \cdot \beta + (\tau')^2 \cdot \beta + ... = \beta \sum_{n=0}^{\infty} (\tau')^n$$

This geometric series can then be rewritten as:

$$R_0 = \beta \cdot \frac{1}{1-\tau'} = \frac{\beta}{\tau} \tag{S1}$$

Phenotyping -- Limitations. The phenotyping procedure enables high throughput identification of resistance profiles. Although this method is generally reliable and effective for most wells, it is difficult to accurately determine the resistance profile for wells with very low bacterial densities

due to the potential for stochastic effects. We analysed 1784 A_r turnover wells treated with antibiotic B during the maximum-emergence scenario. Here, we observed, alongside the expected A_r and U wells, 9% 'other' and 17% S wells, as detailed in Fig. 2.9a. It might be tempting to interpret the S wells as those in which all bacteria lost their plasmids and the 'other' wells as artefacts of measurement errors. Although these interpretations are not incorrect, a more critical factor influencing the measured resistance profile distribution is the inherent stochasticity of the method if applied to low-density wells.

As an example, we will analyse wells identified as A_r-wells during the previous transfer and subsequently treated with antibiotic B. To simplify the following analysis, we only consider agar plates treated with drug $\vartheta \in \{N, A\}$ (no drug, drug A) and disregard plates treated with drug B (B-plates) and AB (AB-plates). Furthermore, we will use a prime (') to indicate a counter probability ($w' = 1 - w$). Drawing a drop with volume V_{drop} from a well with volume V_{well} leads to a probability $p = \frac{V_{\text{drop}}}{V_{\text{well}}}$ of drawing a specific bacterium. The probability that the drawn drop contains no bacteria of phenotype $\psi \in \{\emptyset, a\}$ (without resistance and A-resistance) is $d'_\psi = (1-p)^{Z_\psi}$, with Z_ψ representing the number of bacteria with phenotype ψ inside the well. We denote the probability that a drop can grow on a plate treated with drug ϑ as g_ϑ. The probability g'_N of drawing a drop that will not form a colony on an N-plate can than be defined as $g'_N = d'_\emptyset d'_a$, and the probability g'_A of drawing a drop that will not grow on an A-plate is $g'_A = d'_a$.

Assuming that the drawn drop does not significantly alter the well volume and composition, we obtain the following probabilities for the possible resistance profiles (see also Fig. 2.9b):

$$\mathbb{P}(U) = g'_N \cdot g'_A$$
$$\mathbb{P}(S) = g_N \cdot g'_A$$
$$\mathbb{P}(A_r) = g_N \cdot g_A$$
$$\mathbb{P}(other) = g'_N \cdot g_A$$

Assuming $p = 0.006$ (value for our experiment), a well containing 25 A-resistant and 15 sensitive bacteria will result in 70% U, 26% S, 3% A_r, and 11% other. This result is similar to the experimentally measured distribution (compare Fig. 2.9a).

Advanced Resistance Profiles We introduced advanced phenotypes into our analysis to determine the approximate bacterial density inside the wells. Wells that retain their phenotype after one transfer, despite being sensitive to a particular antibiotic, are expected to exhibit a low bacterial density post-treatment and are labelled ϕ^l. Conversely, wells that were either untreated or treated with an ineffective antibiotic are expected to contain a high bacterial density and are labelled ϕ^h. In addition, wells that underwent a change in resistance profile or were mixed with other wells are denoted as $\phi^?$ and are excluded from further analysis. We summarised the influence of the bacterial densities within the inoculating wells on the frequency of superinfections developing double resistance in Table 2.2.

Statistical Analysis. To compare the performance of different treatment strategies in vitro, we summarized the resistance profiles into groups and focused our analysis on three groups: uninfected, single-resistant and double-resistant. These labels stem from the properties within the wells. That means single resistant wells (A_r, B_r or (A_r&B_r) would be wells that contain only single resistant (or sensitive) bacteria, but no double resistant bacteria and therefore can be cured by combining drugs. In contrast, double-resistant wells cannot be cured using both antibiotics simultaneously since they contain AB-resistant bacteria. We then averaged the frequency of each group over the last four transfers for every replicate. Four transfers correspond to a complete cycle in the cycling strategy with a period of 2 (e.g., A-A-B-B). The effect of the treatment strategy on the average frequencies of uninfected, single-resistant, and double-resistant wells was then tested using a one-way ANOVA. In the case of a significant test ($p < 0.05$), we conducted a pairwise Tukey post hoc analysis to relate the mean frequencies.

In addition, we analysed superinfections between patients and the emergence of double resistance across different strategies in the maximum-emergence scenario. We considered all measurement points from the fourth transfer onwards as at near-stationary level for the non-cycling strategies. Consequently, the initial conditions for each new transfer remain approximately the same or are repeated every fourth transfer in the case of cycling.

For this analysis, we counted the number of newly emerged double-resistant wells $n_{\mathscr{E}}$ and the number of superinfections $n_{\mathscr{S}}$ across all replicates for each plate, with each plate representing one treatment arm for a single transfer. Newly emerged double-resistant wells are defined as those exhibiting double resistance but not having previously been passaged or infected by a

double-resistant well. Additionally, for each plate, we analysed all wells treated with treatment ϑ, counting the number of superinfected wells $n_{\mathscr{S}}^{\vartheta}$ and those among them that developed double resistance $n_{\mathscr{E}}^{\vartheta}$.

We then tested whether the treatment strategy significantly affects the emergence frequency $f_{\mathscr{E}} = n_{\mathscr{E}}/n_P$ and the frequency of superinfection $f_{\mathscr{S}} = n_{\mathscr{S}}/n_P$, with n_P being the number of patients in a hospital ward across all replicates (376) using an ANOVA. Additionally, we used an ANOVA to assess if treatment ϑ significantly influences the frequency of superinfected wells that develop double resistance $n_{\mathscr{E}}^{\vartheta}/n_{\mathscr{S}}^{\vartheta}$.

Subsequent to a significant ANOVA test, we conducted pairwise Tukey post hoc comparisons between the treatment arms ($p < 0.05$).

All statistical analyses were performed in Python 3.8.5 using SciPy's f_oneway() [6] for ANOVA tests and Statsmodels' pairwise_tukeyhsd() [7] for conducting Tukey's honest significant difference post hoc analyses.

***Maximum-emergence* scenario: Predicting the Emergence Probability.** We counted for each plate i the number of superinfected wells $n_{\mathscr{S}}^{i}$ and normalized them by the number of patients per plate n_p to calculate the frequency of superinfection ($f_{\mathscr{S}}^{i} = \frac{n_{\mathscr{S}}^{i}}{n_p}$). Then, we estimated the probability of superinfection $\mathbb{P}(\mathscr{S})$ for each treatment arm by averaging $f_{\mathscr{S}}^{i}$. In addition, we approximated the probability of emergence for superinfected wells $\mathbb{P}_{\vartheta}(\mathscr{E}|\mathscr{S})$ under treatment ϑ, by normalizing the total number of newly emerged resistances across all plates $N_{\mathscr{E}}^{\vartheta}$ by the total number of superinfected wells under treatment ϑ ($N_{\mathscr{S}}^{\vartheta}$): $\frac{N_{\mathscr{E}}^{\vartheta}}{N_{\mathscr{S}}^{\vartheta}}$. The estimates for $\mathbb{P}_{\vartheta}(\mathscr{E}|\mathscr{S})$ were then utilized to approximate the average probability of superinfected wells developing double resistance for each treatment arm. The weighted average of all $\mathbb{P}_{\vartheta}(\mathscr{E}|\mathscr{S})$ were computed using the proportion of patients receiving treatment ϑ as weights. For example, in mixing, the average probability $\overline{\mathbb{P}}(\mathscr{E}|\mathscr{S})$ is given by $0.5\mathbb{P}_A(\mathscr{E}|\mathscr{S}) + 0.5\mathbb{P}_B(\mathscr{E}|\mathscr{S})$. We then used Equation S2 to predict the average probability of emerging double resistance $\mathbb{P}(\mathscr{E})$ for each strategy, as indicated in Figure 3A by black stars.

$$\mathbb{P}(\mathscr{E}) = \mathbb{P}(\mathscr{S})\overline{\mathbb{P}}(\mathscr{E}|\mathscr{S}) \tag{S2}$$

SI Results

Impact of Treatment on the Emergence of Double Resistance. As demonstrated in Figure 3B, our findings indicate that treatment substantially influences the frequency of emerging double resistance in superinfected wells. Population dynamics within wells can potentially explain these results. Here we approximate $\mathbb{E}_\vartheta$, the expected number of conjugations during one treatment phase under treatment ϑ, as $\mathbb{E}_\vartheta \propto \gamma_\vartheta \int_{t1}^{t2} {}^A X_\vartheta(t) {}^B X_\vartheta(t) dt$. ${}^i X$ represents the density of bacteria with resistance i, and γ_ϑ is the treatment dependent conjugation rate. The experimentally generated data are insufficient for adequately estimating γ_ϑ. However, if we assume identical initial bacterial populations, we can qualitatively rank the cumulative product of bacterial densities $\int_{t1}^{t2} {}^A X_\vartheta(t) {}^B X_\vartheta(t) dt$. The highest cumulative product is achieved when ${}^A X$ and ${}^B X$ grow without or with ineffective treatment. Additionally, we know that the clearance rate of ceftazidime (drug A) is substantially higher than that of tetracycline (drug B), as shown in Table 2.9, resulting in a larger cumulative product over time when treated with antibiotic B. Lastly, the lowest cumulative product is associated with treatment AB, where neither of the two strains can grow. Therefore, if we disregard γ_ϑ, the above reasoning predicts the following ranking for the number of emergences per superinfection: None, B, A, AB. This predicted ranking aligns with the ranking observed in Figure 3C.

Another potential explanation are potential differences in the plasmid-specific conjugation rates. If, for example, p_B had a higher conjugate rate than p_A, then drug A would have a stronger impact on the emergence of double resistance, even if we assumed identical clearance rates.

Treatment strategies influence the number of bacteria inoculating superinfections. We observed that the number of single-resistant bacteria that inoculate superinfections affects the emergence of double resistance (Table 2.2). At least one of the two superinfection-initiating inocula originates from infections between patients and is sourced from the previous assay plate. The cell densities and compositions within these source wells, which have already undergone treatment for one day, vary considerably depending on the resistance profile ϕ and the treatment history. We used 'advanced phenotypes' (see SI Methods) to distinguish between high-density (ϕ^h) and low-density (ϕ^l) wells, assigning these based on the wells resistance profile (ϕ) and treatment history.

During the maximum-emergence scenario, which contained the highest number of superinfections, we made two noteworthy observations. First, superinfections between ϕ^h and ϕ^l ($A_r^l + B_r^h$ (43 superinfections) and $A_r^h + B_r^l$ (one superinfection)) occur significantly less frequently than superinfections between $A_r^h + B_r^h$ (a total of 1176 superinfections, as outlined in Table 2.2). This discrepancy can be attributed to the high clearance rates of both drugs, resulting in a higher prevalence of ϕ^h compared to ϕ^l.

Second, none of the 44 superinfections involving $A_r^l + B_r^h$ and $A_r^h + B_r^l$ resulted in double resistance.

Antagonism. Adding the bacteriostatic antibiotic tetracycline (drug B) reduces the probability of clearing sensitive bacteria with the bactericidal antibiotic ceftazidime (drug A). The clearance probability drops from 0.97 to 0.86, as shown in Table 2.9. Antagonism between bactericidal and bacteriostatic antibiotics has been documented by various researchers since the 1950s, as exemplified by the works of Cates [8] and Jawetz [9], and also more recently by Ocampo [10]. The antagonistic effect may arise because the bacteriostatic drug (tetracycline) lowers the growth rate, resulting in a decreased kill rate of the bactericidal drug (ceftazidime) [11]. Accordingly, this antagonistic effect is anticipated to be less pronounced for a tetracycline-resistant strain, where the impact on the growth rate is diminished. This hypothesis is supported by the measured clearance rates for B_r wells, where the clearance probability remains at 0.98 for treatment with drugs A and AB Table 2.9.

SI Computational Model

Stochasticity We conducted three experiments, each defined by one parameter set consisting of a turnover probability τ, an infection probability β and the probability distribution for sampling patients c_ϕ with different resistance profiles $\phi \in \{U, S, A_r, B_r, AB_r\}$. For each experiment, we randomly generated one instruction set based on the given parameter set. Due to the scale and complexity of the experiment, it was infeasible to conduct a unique instruction set for each replicate. Therefore, we opted to employ identical instruction sets for all replicates, which reduces the number of robot arm movements (and time) for infection and turnover by a factor of four.

As a consequence, our replicates may be interpreted as patients with identical histories regarding original infection, treatment and exchange with other patients. However, due to the accumulated biological stochasticity along the patient histories, their phenotypic properties may vary, as

reflected by the variance of the replicates.

Since we only tested one instruction set per replicate in vitro, we wondered whether the measured results depend on the randomisation of the instruction set and if we would expect a qualitatively different result if we reran the experiment 100 times. To answer this question, we created a computational model that, for a given parameter set, rerandomises the instruction set and conducts a stochastic simulation to mimic the biological variability. In Fig. 2.7, we visualised the different sources of experimental and computational variability.

Transition Probabilities. We used the experimental data to calculate the transition frequencies for all pre-treatment $\phi_\vartheta^i(T)$ to post-treatment $\phi_\vartheta^i(\hat{T})$ resistance profile combinations for each plate i and treatment ϑ. $\phi(\hat{T})$ is measured during the phenotyping procedure, while $\phi(T)$ is estimated by employing one plate-handling simulation step to $\phi(\hat{T}-1)$ as described in the methods (e.g. $A_r+S \rightarrow A_r$). Then, we estimated the transition probabilities as the weighted average of transition frequencies across all plates, with the count of $\phi_\vartheta(T)$ on each plate as a weight.

For each treatment ϑ, we created one transition matrix M^ϑ, with the pre-treatment resistance profile $\phi(T)$ as columns and the post-treatment profile $\phi(\hat{T})$ in the rows (Table 2.19–2.22). To simulate the incubation phase, we use M^ϑ to stochastically assign the post-treatment resistance profile $\phi_\vartheta(\hat{T})$, using the respective column of the transition matrix as a probability distribution.

Transition Probabilities for Transfer 1. All patients are untreated during transfer 0, leading to exceptionally high rates of superinfections and high emergence rates per superinfection during transfer 1. To account for this, we created four additional transition matrices for simulating the first transfer (see Table 2.23–2.26).

Choice of Model. We also considered using a continuous model. However, a typical population-based model would not match the experimental measurements for effectively treated patients. This is due to the discrete nature of our experimental setup. Here, the frequency of infected patients has a local maximum before treatment and a local minimum after treatment, creating sawtooth-shaped frequencies over time. We conducted the phenotyping at the end of the incubation period, at the local low point, diverging from the average frequencies predicted by a continuous model. Therefore, a continuous model would either use realistic clearance rates and

not fit through the experimental data points or use exaggerated clearance rates and fit through the data points. For example, treating an S well with a hypothetical drug C leads to a steady decline in bacterial density over time, resulting in a bacterial density below the detection limit after 24 hours (our first experimental measurement point). If initially, all wells are infected, and at the first measurement point, the infection drops to 0%, fitting a continuous compartmental model to these data would result in infinite clearance rates.

Contamination of the Transition Matrix. The computational simulations employ four transition matrices ($M^{\text{none}}, M^{A}, M^{B}, M^{AB}$) derived from the observed transitions during the three experiments. During the experiments, we observed a low rate of contamination affecting neighbouring wells, likely due to pintool and plate movements by the liquid handling platform. Quantifying the exact contamination rate is challenging, though the observed mean transition probability from U to U is 0.99%.

These contaminations can be inconsequential; for example, an S well contaminating an A_r well will not cause a shift of the resistance profile in the contaminated well. However, they can also lead to artefactual transitions that are reflected in the transition matrices, such as $U \rightarrow S$ (Table 2.19), $U \rightarrow A_r$ (Table 2.20), or $U \rightarrow B_r$ (Table 2.21). The impact of the recorded artefactual transitions in the transition matrices depends on the frequency and the transferred resistance profile. For instance, in Mono A, a high frequency of A_r contaminations is observed due to the predominant presence of A_r wells, creating the impossible transition $U \rightarrow A_r$ described above, which now occurs in all simulations independent of the presence or frequency of A_r during the simulation. Similarly, in the containment experiment, the abundance of AB_r wells in all treatment arms led to a higher rate of double-resistant contamination reflected in the transitions: $A_r \rightarrow AB_r$ (Table 2.19) and $A_r \rightarrow AB_r$ & $B_r \rightarrow AB_r$ (Table 2.21). Resistance mutations could also explain these transitions; however, because they occurred mainly during the containment scenario and the fact that they exclusively came up in wells neighbouring double-resistant wells, we believe that they are an artefact of unintended infections.

Artefactual transitions such as $U \rightarrow S$, or $U \rightarrow A_r$ have a neglectable effect on the simulation of all scenarios, as their occurrence in the regular infection and admission processes outweighs the contribution through the artefactual transitions. Similarly, double-resistant contaminations minimally impact the simulations of both the containment scenario (where double resistance

is regularly admitted) and the maximum-emergence scenario (due to a low R_0 and frequent emergence of double resistance). However, they pose a problem to the simulation of prevention scenario, where a low (untruthful) influx of AB_r can spread ($R_0 > 1$).

Filtered Transition Probabilities. To mitigate the effect of contaminated transition matrices, we introduced filtered transition matrices. For this, we assumed no resistance mutations and forbidding impossible transitions (by setting the transition probability $U \rightarrow U$ to 1; see Table 2.27 – 2.34).

Using these filtered probabilities to simulate the prevention scenario leads to better-matching results, almost removing the spread of double resistance in Mono A and the multidrug strategies and thereby matching the experimental data better (compare the green error bands between Fig. 2.6 & Fig. 2.11). In addition, we conducted a secondary sensitivity analysis with these filtered probabilities (see Fig. 2.12). Because the overall conclusions are consistent between the simulations using filtered and unfiltered transition probabilities, we opted to use the unfiltered transition probabilities in the main paper for a more direct representation of the experimental data.

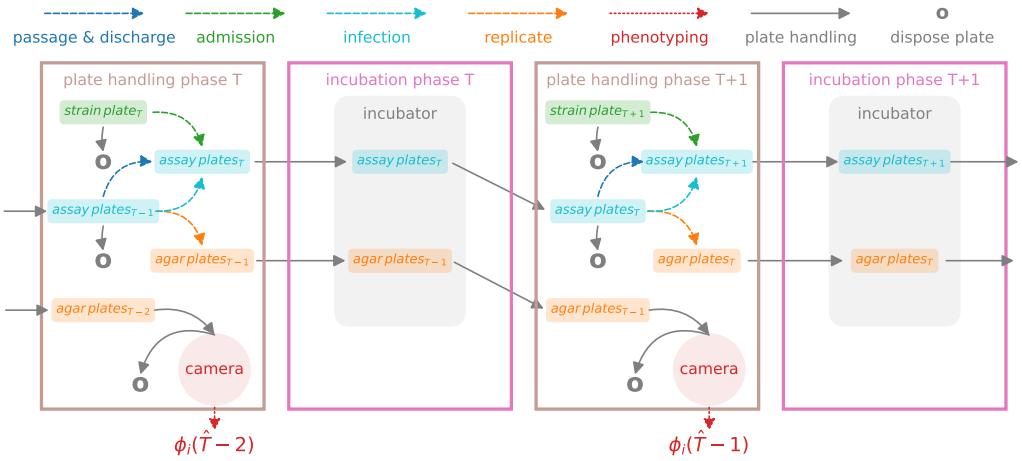

Fig. 2.5 Schematic illustrating the procedure used in the experiment for transfers T and T+1 in the liquid handling platform after adding medium and drugs to the assay plates. Every transfer (day), we provide new assay and agar plates. Plates from the previous transfers are removed. To inoculate the new assay plates with newly admitted patients from the strain plate, along with staying patients and infection between patients from the previous assay plate, we use a pintool with retractable pins (dashed lines). Discharged patients are not transferred (pins retracted) to the new assay plates. Plates are then automatically transferred (solid lines) to the incubator for overnight incubation. Subsequently, we replicate each assay plate onto four agar plates using the pintool. These plates are treated with antibiotics A, B, and AB, and one remains untreated. Once the agar plates have been incubated overnight, we capture images (dotted lines) to determine the resistance profile ϕ_i for each well i.

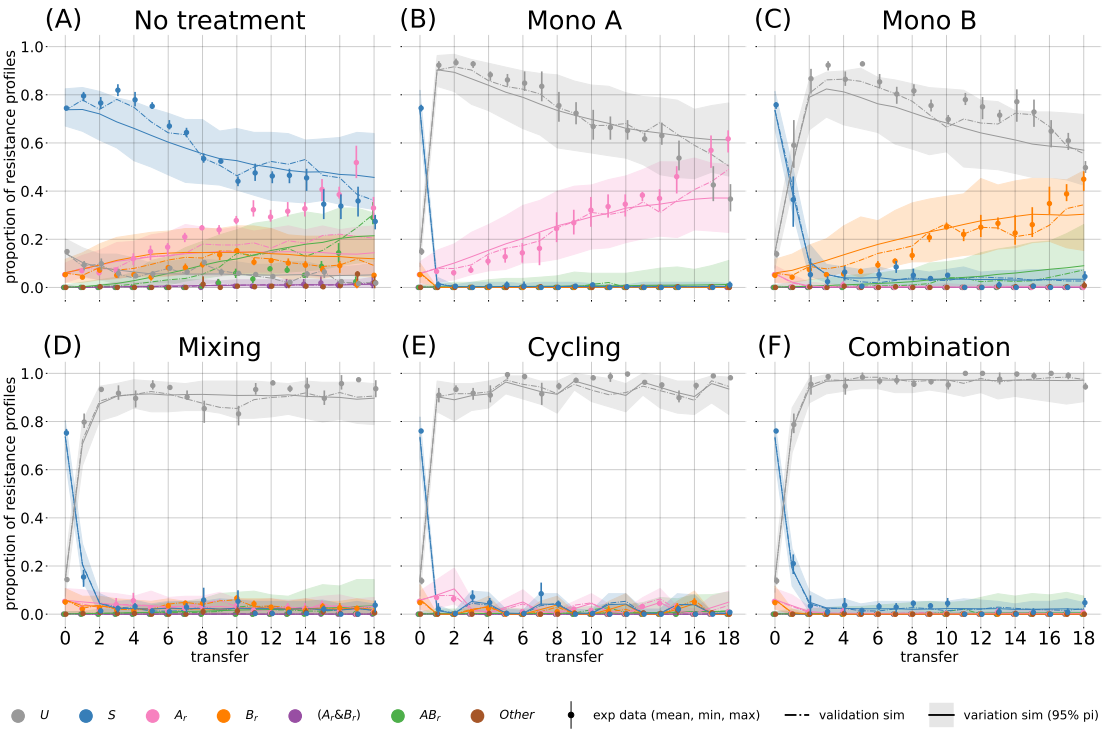

Fig. 2.6 Prevention scenario: Frequencies of resistance profiles (colours) over time during the prevention scenario. The dots show the experimental measurements, and the error bar indicates the min/max interval between the replicates. The dash-dotted line shows the mean value of 100 stochastic simulations based on the instruction set used in the in vitro experiment. The solid line represents the mean value of 100 simulations with randomly created instruction sets based on the parameter set used in the experiment. The shaded error band indicates the 95-percentile interval between the simulations.

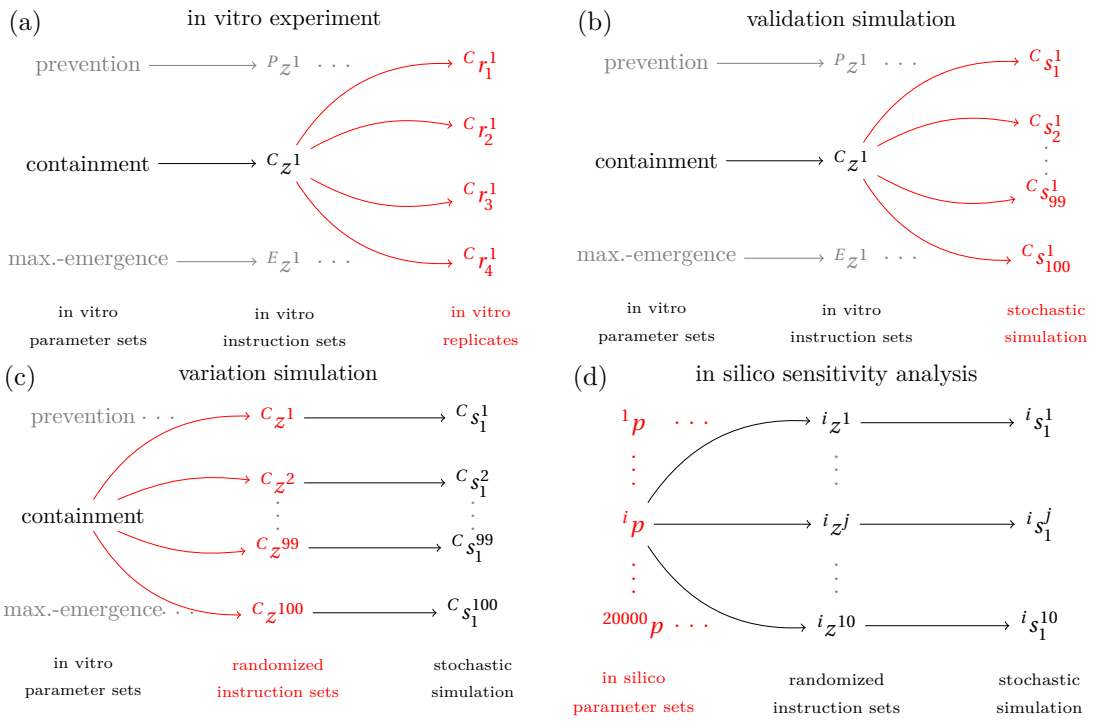

Fig. 2.7 Illustration depicting the various sources of stochasticity and variation in experiments and simulations. Our experiments and simulations investigate various sources of stochasticity and their contributions to the variability of the outcome. In panels A-D, we sketch the different sources of stochasticity for each experiment and simulation, highlighting our primary focus in red. (A) In vitro Experiment. Each experiment explores a scenario and is defined by a distinct parameter set (prevention (P), containment (C), maximum emergence (E)). We randomly generated one instruction set for each parameter set i: ${}^{i}z^{1}$. For each instruction set ${}^{i}z^{1}$, we replicated the cumulative in-well dynamics four times ${}^{i}r_{j}^{1}$. (B) Validation Simulation. To assess our computational model, we employed identical parameter sets and instruction sets ${}^{i}z^{1}$, as employed in the in vitro experiments. For each instruction set ${}^{i}z^{1}$, we conducted 100 stochastic simulations ${}^{i}s_{j}^{1}$. (C) Variation Simulation. For every in vitro parameter set, we randomly generated 100 alternative instruction sets ${}^{i}z^{k}$ to quantify the influence of experimental decisions on the experiment's outcomes. For each instruction set, we performed one simulation ${}^{i}s_{1}^{k}$. (D) In Silico Sensitivity Analysis. We examined the sensitivity of our experimental findings to the input parameters by examining the effects of varying the input parameters on the resulting frequency of uninfected cases for different treatment strategies. To achieve this, we generated 20,000 alternative parameter sets ${}^{i}p$. We created ten randomised instruction sets ${}^{i}z^{k}$ for each parameter set ${}^{i}p$ and simulated each instruction set one time (${}^{i}s_{1}^{k}$).

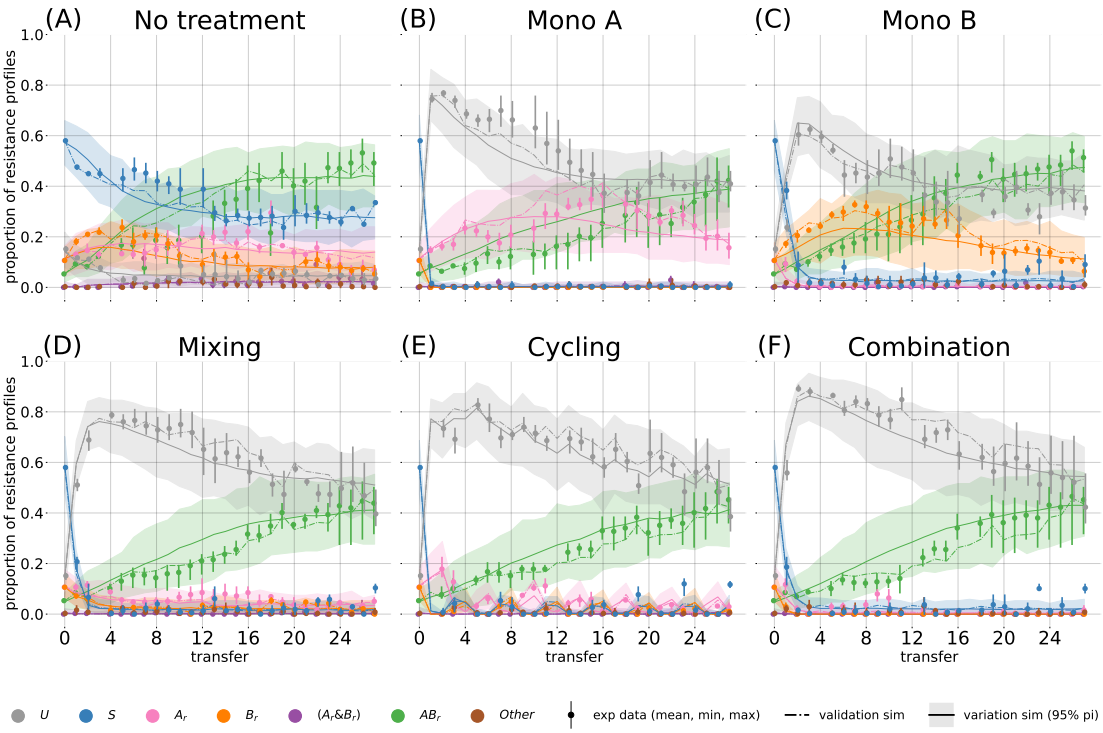

Fig. 2.8 Containment scenario: Frequencies of resistance profiles (colours) over time during the containment scenario. The dots show the experimental measurements, and the error bar indicates the min/max interval between the replicates. The dash-dotted line shows the mean value of 100 stochastic simulations based on the instruction set used in the in vitro experiment. The solid line represents the mean value of 100 simulations with randomly created instruction sets based on the parameter set used in the experiment. The shaded error band indicates the 95-percentile interval between the simulations.

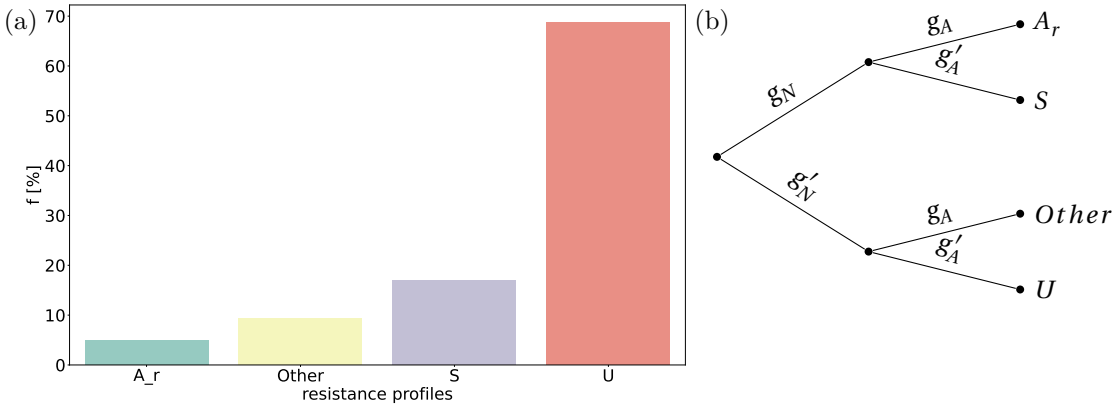

Fig. 2.9 (A) Experimentally measured resistance profiles for 1784 wells with the pre-treatment profile A_r and treatment with drug B during the maximum-emergence scenario. (B) Decision tree to calculate the distribution of measured phenotypes for a well that contains $Z_\emptyset$ sensitive and Z_A A-resistant bacteria. g_ϑ is the probability of drawing a drop that forms a colony on a plate treated with drug ϑ, while g'_ϑ is the probability that it does not form a colony.

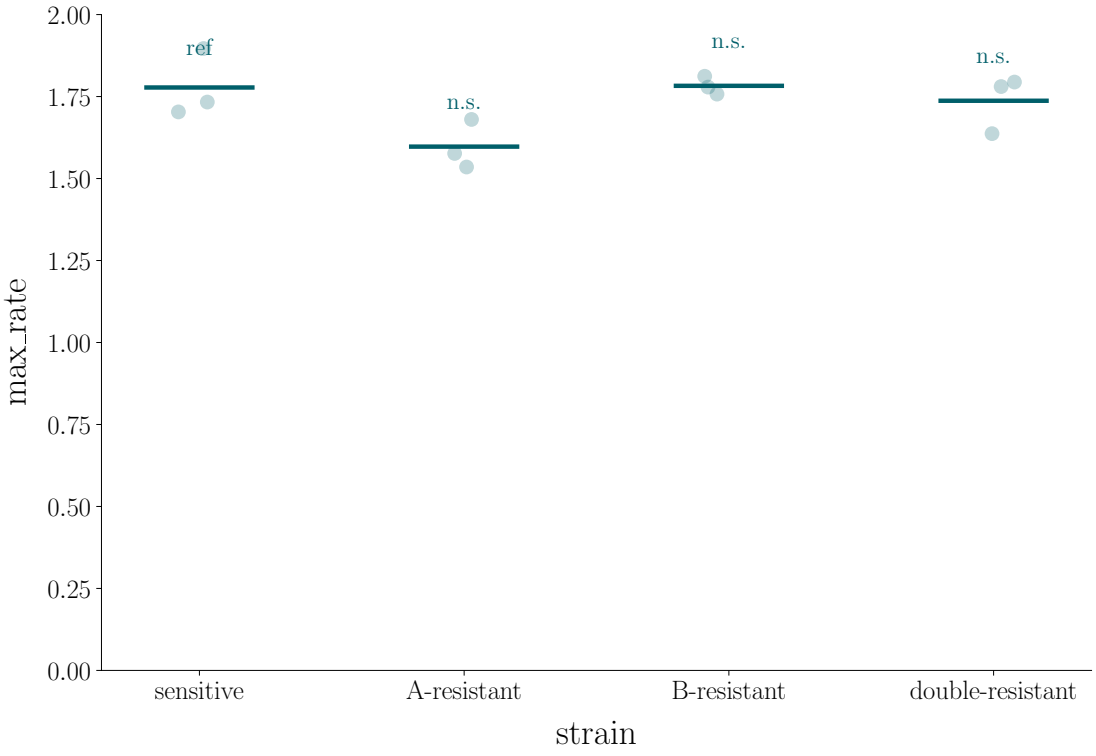

Fig. 2.10 Maximum growth rates of sensitive and plasmid-carrying strains, measured using OD-growth curves. Each dot represents an individual well, and vertical bars indicate the mean. The sensitive strain was used as the reference ("ref") for pairwise comparisons to the plasmid-carrying strains to identify potential plasmid costs. We used the Mann-Whitney U tests with the Bonferroni correction to identify significant differences in growth rates. All pairwise comparisons were not significant (n.s.).

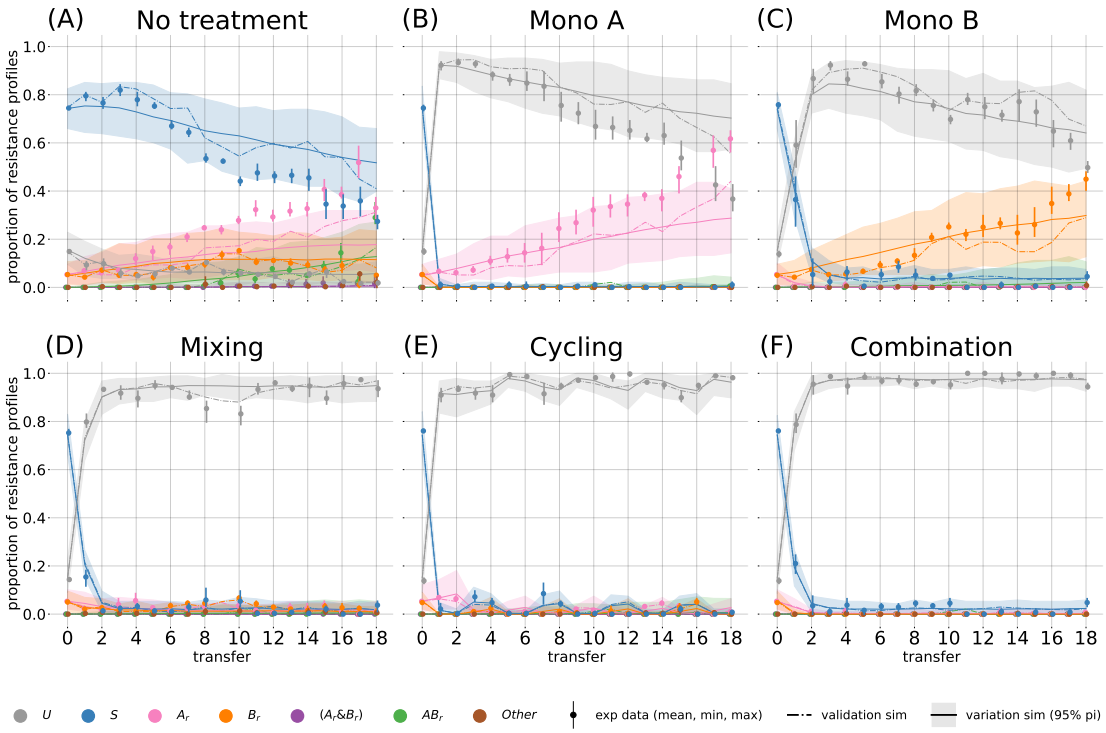

Fig. 2.11 Prevention scenario with filtered transition probabilities. Frequencies of resistance profiles (colours) over time during the prevention scenario. The dots show the experimental measurements, and the error bar indicates the min/max interval between the replicates. The dash-dotted line shows the mean value of 100 stochastic simulations based on the instruction set used in the in vitro experiment. The solid line represents the mean value of 100 simulations with randomly created instruction sets based on the parameter set used in the experiment. The shaded error band indicates the 95-percentile interval between the simulations.

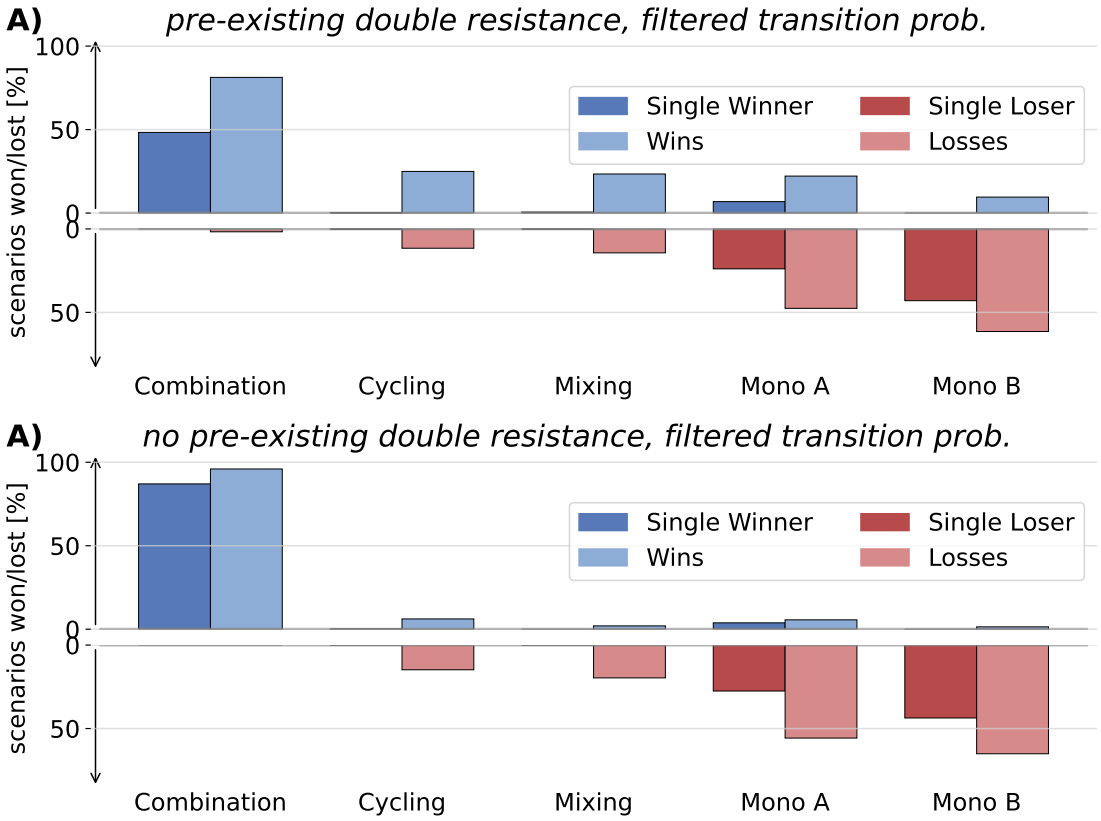

Fig. 2.12 Sensitivity analysis using filtered transition probabilities. We evaluated the effectiveness of the five treatment strategies in maximising the frequency of uninfected in silico patients across randomly generated parameter sets. Strategies not significantly better than any other are marked as losers (pastel red), with those significantly worse than all others being labelled as single losers (dark red). Conversely, strategies that are not significantly worse than any other are classified as winners (pastel blue), and those significantly better than all others as single winners (dark blue). (A) Evaluation of 10,000 parameter sets with preexisting double resistance. 659 out of 10,000 parameter sets yielded no significant difference between the strategies. (B) Evaluation of 10,000 parameter sets without preexisting double resistance. 8 out of 10,000 parameter sets yielded no significant difference between the strategies.

Table 2.2 Number of superinfections ($N_{\mathscr{S}}$) between high- and low-concentrated A_r and B_r wells and the number of double resistances that emerged ($N_{\mathscr{E}}$) under treatment ϑ across all three experiments.

Treatment ϑ	$\mathbf{A_r^x}$	$\mathbf{B_r^x}$	$\mathbf{N_{\mathscr{E}}^{\vartheta}}$	$\mathbf{N_{\mathscr{S}}^{\vartheta}}$	$\frac{\mathbf{N_{\mathscr{E}}^{\vartheta}}}{\mathbf{N_{\mathscr{S}}^{\vartheta}}}$
A	A_r^h	B_r^h	55	399	0.14
AB	A_r^h	B_r^h	2	35	0.06
B	A_r^h	B_r^h	257	322	0.8
none	A_r^h	B_r^h	390	420	0.93
A	A_r^h	B_r^l	0	1	0.0
A	A_r^l	B_r^h	0	13	0.0
AB	A_r^l	B_r^h	0	15	0.0
B	A_r^l	B_r^h	0	15	0.0

Table 2.3 Strains used in this study and their relevant phenotypes. The phenotype in brackets is conferred by the respective plasmid. Cm^R: Chloramphenicol resistance, Amp^R: Ampicillin resistance, Caz^R: Ceftazidime resistance, Tet^R: Tetracycline resistance.

Name	Relevant phenotype	Reference
Escherichia coli MDS42-YFP;Cm^R;[3] A-resistant	Cm^R pA (Amp^R, Caz^R)	this study, [2
B-resistant	Cm^R pB (Amp^R, Tet^R)	this study, [2
AB-resistant	Cm^R pA (Amp^R, Caz^R) pB (Amp^R, Tet^R)	this study, [2

Table 2.4 Statistical comparison of maximum growth rates between the sensitive and plasmid-carrying strains. We used a Mann-Whitney U test for pairwise comparisons, and the p-values were adjusted using the Bonferroni correction.

Comparison	U-statistic	P-value	Corrected P-value	Significant after Bonferroni
sensitive vs A-resistant	9.000000	0.100000	0.300000	False
sensitive vs B-resistant	3.000000	0.700000	1.000000	False
sensitive vs double-resistant	5.000000	1.000000	1.000000	False

Table 2.5 Plasmid segregation loss was estimated over 24 hours without treatment and with selective treatment as a control. Frequencies of plasmid retention were compared between t_0 – t_1 using the Mann-Whitney U test. Confidence intervals and the mean frequencies were estimated by bootstrapping the binary data (plasmid retained or lost) pooled across replicates. No significant plasmid loss was observed in either the main data or the control.

plasmids	$f(t_0)$	$CI(t_0)$	$f(t_1)$	$CI(t_1)$	p-value	$f(t_1)$ control	$CI(t_1)$ control	p-value control
p_A	1.00	(1.0, 1.0)	1.00	(1.0, 1.0)	1.00	1.00	(1.0, 1.0)	1.00
p_B	1.00	(1.0, 1.0)	0.97	(0.93, 1.0)	0.20	1.00	(1.0, 1.0)	1.00
p_A&p_B	0.99	(0.97, 1.0)	1.00	(1.0, 1.0)	0.50	1.00	(1.0, 1.0)	0.50

Table 2.6 95 % confidence intervals for the final bacterial density measured by colony plating and the maximal growth rates measured by evaluating OD-growth curves.

strain	antibiotic	cmp $[\mu g/ml]$	cfu $[1/\mu l]$	growthrate $[1/h]$
double-resistant	AB	5	$(2.14-3.33)\times 10^5$	$(0.43-0.86)$
double-resistant	AB	25	$(2.68-3.99)\times 10^5$	$(0.4-0.85)$
A-resistant	A	5	$(1.58-2.62)\times 10^5$	$(0.51-0.7)$
A-resistant	A	25	$(2.05-3.21)\times 10^5$	$(0.46-0.71)$
sensitive	None	5	$(1.03-1.27)\times 10^6$	$(0.68-0.74)$
sensitive	None	25	$(1.15-1.4)\times 10^6$	$(0.55-0.96)$
B-resistant	B	5	$(4.05-5.62)\times 10^5$	$(0.45-0.74)$
B-resistant	B	25	$(3.53-5.01)\times 10^5$	$(0.4-0.87)$

Table 2.7 Definition of resistance profiles (rows) by growth patterns on differently treated agar plates (columns). X indicates colony formation, whereas o indicates no growth.

	None	A	B	AB
U	o	o	o	o
S	X	o	o	o
A_r	X	X	o	o
B_r	X	o	X	o
$(A_r\&B_r)$	X	X	X	o
AB_r	X	X	X	X

Table 2.8 Association between bacterial phenotypes (rows) and resistance profiles ϕ (columns). An 'X' denotes that a phenotype is obligatory for a given profile, while a '$\surd$' indicates that it is optional.

	U	S	A_r	B_r	$(A_r\&B_r)$	AB_r
sensitive		X	$\surd$	$\surd$	$\surd$	$\surd$
A-resistant			X		X	$\surd$
B-resistant				X	X	$\surd$
double-resistant						X

Table 2.9 Clearance probability of well phenotypes across the three experiments.

	S	A_r	B_r
A	0.97	0.02	0.98
B	0.73	0.62	0.01
AB	0.86	0.4	0.98

Table 2.10 Mixing rules. During the plate-handling phase, we mix wells due to infections. The resulting phenotype of the two mixed wells can be calculated using this table. More than two phenotypes can be combined by applying associative logic.

$\phi_1(\hat{T})$ \ $\phi_2(\hat{T})$	U	S	A_r	B_r	$(A_r\&B_r)$	AB_r
U	U	S	A_r	B_r	$(A_r\&B_r)$	AB_r
S	S	S	A_r	B_r	$(A_r\&B_r)$	AB_r
A_r	A_r	A_r	A_r	$(A_r\&B_r)$	$(A_r\&B_r)$	AB_r
B_r	B_r	B_r	$(A_r\&B_r)$	B_r	$(A_r\&B_r)$	AB_r
(A_r&B_r)	$(A_r\&B_r)$	$(A_r\&B_r)$	$(A_r\&B_r)$	$(A_r\&B_r)$	$(A_r\&B_r)$	AB_r
AB_r	AB_r	AB_r	AB_r	AB_r	AB_r	AB_r

Table 2.11 Mean parameter leading to n single wins during the sensitivity analysis without preexisting double resistance. Strategies that did not yield at least one single win were excluded.

	turnover	infection	U	S	A_r	B_r	AB_r	n
Combination	0.50	0.50	0.26	0.24	0.24	0.25	0.00	9311.00
Mono A	0.80	0.27	0.26	0.29	0.37	0.08	0.00	56.00
Cycling	0.10	0.39	0.33	0.42	0.14	0.10	0.00	4.00
Mixing	0.11	0.33	0.12	0.49	0.38	0.01	0.00	1.00

Table 2.12 Mean parameter leading to n single losses during the sensitivity analysis without preexisting double resistance. Strategies that did not yield at least one single loss were excluded.

	turnover	infection	U	S	A_r	B_r	AB_r	n
Mono B	0.60	0.43	0.26	0.25	0.16	0.33	0.00	4132.00
Mono A	0.55	0.43	0.27	0.25	0.36	0.12	0.00	2648.00
Cycling	0.07	0.87	0.28	0.34	0.27	0.11	0.00	8.00
Mixing	0.07	0.90	0.69	0.25	0.01	0.05	0.00	1.00

Table 2.13 Mean parameter leading to n single wins during the sensitivity analysis with preexisting double resistance. Strategies that did not yield at least one single win were excluded.

	turnover	infection	U	S	A_r	B_r	AB_r	n
Combination	0.61	0.47	0.21	0.18	0.22	0.22	0.17	5487.00
Mono A	0.52	0.56	0.23	0.20	0.16	0.15	0.26	365.00
Mixing	0.13	0.30	0.23	0.21	0.18	0.15	0.22	40.00
Cycling	0.14	0.20	0.23	0.20	0.21	0.20	0.16	9.00

Table 2.14 Mean parameter leading to n single losses during the sensitivity analysis with preexisting double resistance. Strategies that did not yield at least one single loss were excluded.

	turnover	infection	U	S	A_r	B_r	AB_r	n
Mono B	0.57	0.46	0.21	0.19	0.13	0.28	0.18	4250.00
Mono A	0.51	0.43	0.23	0.19	0.30	0.10	0.18	2359.00
Cycling	0.42	0.72	0.23	0.21	0.14	0.14	0.28	6.00
Mixing	0.34	0.71	0.23	0.20	0.18	0.09	0.30	2.00

Table 2.15 Wins and losses during the sensitivity analysis. With preexisting double resistance. 606 parameter sets yielded an insignificant result.

strategy	single winner [%]	single loser [%]	loser [%]	winner [%]	single winner	single loser	loser	winner
Combination	54.87	0.00	0.95	86.76	5487	0	95	8676
Cycling	0.09	0.06	12.10	23.32	9	6	1210	2332
Mixing	0.40	0.02	14.78	20.54	40	2	1478	2054
Mono A	3.65	23.59	48.57	17.49	365	2359	4857	1749
Mono B	0.00	42.50	62.29	8.11	0	4250	6229	811

Table 2.16 Wins and losses during the sensitivity analysis without preexisting double resistance. 100 parameter sets yielded an insignificant result.

strategy	single winner [%]	single loser [%]	loser [%]	winner [%]	single winner	single loser	loser	winner
Combination	93.11	0.00	0.00	98.35	9311	0	0	9835
Cycling	0.04	0.08	18.89	3.49	4	8	1889	349
Mixing	0.01	0.01	22.05	1.32	1	1	2205	132
Mono A	0.56	26.48	57.03	1.65	56	2648	5703	165
Mono B	0.00	41.32	63.44	1.11	0	4132	6344	111

Table 2.17 Wins and losses during the sensitivity analysis, using filtered transition probabilities and preexisting double resistance. 659 parameter sets yielded an insignificant result.

strategy	single winner [%]	single loser [%]	loser [%]	winner [%]	single winner	single loser	loser	winner
Combination	48.31	0.00	1.72	81.27	4831	0	172	8127
Cycling	0.07	0.10	11.57	24.94	7	10	1157	2494
Mixing	0.59	0.03	14.34	23.40	59	3	1434	2340
Mono A	6.85	23.91	47.57	22.15	685	2391	4757	2215
Mono B	0.00	42.97	61.45	9.57	0	4297	6145	957

Table 2.18 Wins and losses during the sensitivity analysis with filtered transition matrices and no preexisting double resistance. 8 parameter sets yielded an insignificant result.

strategy	single winner [%]	single loser [%]	loser [%]	winner [%]	single winner	single loser	loser	winner
Combination	87.04	0.00	0.00	95.98	8704	0	0	9598
Cycling	0.08	0.06	14.80	6.16	8	6	1480	616
Mixing	0.00	0.04	19.66	2.00	0	4	1966	200
Mono A	3.82	27.53	55.71	5.62	382	2753	5571	562
Mono B	0.00	43.67	65.10	1.41	0	4367	6510	141

Table 2.19 M^{none}. Unfiltered transition matrix for untreated wells.

$\phi(\hat{T})$ \ $\phi(T)$	U	S	A_r	B_r	$(A_r\&B_r)$	AB_r
U	0.97	0.0	0.0	0.0	0.0	0.0
S	0.03	0.98	0.01	0.02	0.01	0.01
A_r	0.0	0.01	0.96	0.0	0.07	0.03
B_r	0.0	0.01	0.0	0.97	0.02	0.0
(A_r&B_r)	0.0	0.0	0.01	0.01	0.08	0.04
AB_r	0.0	0.0	0.02	0.0	0.82	0.92

Table 2.20 M^{A}. Unfiltered transition matrix for wells treated with antibiotic A.

$\phi(\hat{T})$ \ $\phi(T)$	U	S	A_r	B_r	$(A_r\&B_r)$	AB_r
U	0.99	0.96	0.02	0.97	0.03	0.02
S	0.0	0.02	0.0	0.01	0.0	0.0
A_r	0.01	0.02	0.98	0.01	0.59	0.01
B_r	0.0	0.0	0.0	0.01	0.0	0.0
(A_r&B_r)	0.0	0.0	0.0	0.0	0.18	0.01
AB_r	0.0	0.0	0.0	0.0	0.2	0.96

Table 2.21 M^{B}. Unfiltered transition matrix for wells treated with antibiotic B.

$\phi(\hat{T})$ \ $\phi(T)$	U	S	A_r	B_r	$(A_r\&B_r)$	AB_r
U	0.99	0.8	0.63	0.01	0.03	0.02
S	0.0	0.19	0.18	0.0	0.0	0.0
A_r	0.0	0.0	0.18	0.0	0.0	0.0
B_r	0.01	0.01	0.0	0.98	0.21	0.0
(A_r&B_r)	0.0	0.0	0.0	0.0	0.03	0.0
AB_r	0.0	0.0	0.01	0.01	0.73	0.98

Table 2.22 M^{AB}. Unfiltered transition matrix for wells treated with antibiotic AB.

$\phi(\hat{T})$ \ $\phi(T)$	U	S	A_r	B_r	$(A_r\&B_r)$	AB_r
U	1.0	0.9	0.49	0.98	1.0	0.02
S	0.0	0.1	0.32	0.02	0.0	0.0
A_r	0.0	0.0	0.19	0.0	0.0	0.0
B_r	0.0	0.0	0.0	0.0	0.0	0.0
(A_r&B_r)	0.0	0.0	0.0	0.0	0.0	0.0
AB_r	0.0	0.0	0.0	0.0	0.0	0.98

Table 2.23 M_1^{none}. Unfiltered transition matrix for the first time point in untreated wells.

$\phi(\hat{T})$ \ $\phi(T)$	U	S	A_r	B_r	$(A_r\&B_r)$	AB_r
U	0.96	0.0	0.0	0.0	0.0	0.0
S	0.03	0.99	0.0	0.0	0.0	0.0
A_r	0.01	0.01	1.0	0.0	0.0	0.0
B_r	0.0	0.0	0.0	1.0	0.17	0.0
(A_r&B_r)	0.0	0.0	0.0	0.0	0.02	0.0
AB_r	0.0	0.0	0.0	0.0	0.81	1.0

Table 2.24 M_1^{A}. Unfiltered transition matrix for the first time point in wells treated with antibiotic A.

$\phi(\hat{T})$ \ $\phi(T)$	U	S	A_r	B_r	$(A_r\&B_r)$	AB_r
U	0.99	0.97	0.0	0.99	0.23	0.0
S	0.0	0.02	0.0	0.01	0.0	0.0
A_r	0.01	0.01	1.0	0.0	0.54	0.0
B_r	0.0	0.0	0.0	0.0	0.0	0.0
(A_r&B_r)	0.0	0.0	0.0	0.0	0.11	0.0
AB_r	0.0	0.0	0.0	0.0	0.12	1.0

Table 2.25 M_1^{B}. Unfiltered transition matrix for the first time point in wells treated with antibiotic B.

$\phi(\hat{T})$ \ $\phi(T)$	U	S	A_r	B_r	$(A_r\&B_r)$	AB_r
U	1.0	0.48	0.51	0.02	0.01	0.0
S	0.0	0.52	0.21	0.01	0.0	0.0
A_r	0.0	0.0	0.28	0.0	0.0	0.0
B_r	0.0	0.0	0.0	0.97	0.31	0.0
(A_r&B_r)	0.0	0.0	0.0	0.0	0.1	0.0
AB_r	0.0	0.0	0.0	0.0	0.58	1.0

Table 2.26 M_1^{AB}. Unfiltered transition matrix for the first time point in wells treated with antibiotic AB.

$\phi(\hat{T})$ \ $\phi(T)$	U	S	A_r	B_r	$(A_r\&B_r)$	AB_r
U	0.98	0.79	0.32	0.67	0.24	0.0
S	0.02	0.21	0.21	0.24	0.21	0.0
A_r	0.0	0.0	0.47	0.0	0.41	0.0
B_r	0.0	0.0	0.0	0.09	0.02	0.0
(A_r&B_r)	0.0	0.0	0.0	0.0	0.07	0.0
AB_r	0.0	0.0	0.0	0.0	0.05	1.0

Table 2.27 M^{none}. Filtered transition matrix for untreated wells.

$\phi(\hat{T})$ \ $\phi(T)$	U	S	A_r	B_r	$(A_r\&B_r)$	AB_r
U	1.0	0.0	0.0	0.0	0.0	0.0
S	0.0	1.0	0.01	0.02	0.01	0.01
A_r	0.0	0.0	0.99	0.0	0.07	0.03
B_r	0.0	0.0	0.0	0.98	0.02	0.0
(A_r&B_r)	0.0	0.0	0.0	0.0	0.08	0.04
AB_r	0.0	0.0	0.0	0.0	0.82	0.92

Table 2.28 M^{A}. Filtered transition matrix for wells treated with antibiotic A.

$\phi(\hat{T})$ \ $\phi(T)$	U	S	A_r	B_r	$(A_r\&B_r)$	AB_r
U	1.0	0.98	0.02	0.98	0.03	0.02
S	0.0	0.02	0.0	0.01	0.0	0.0
A_r	0.0	0.0	0.98	0.0	0.59	0.01
B_r	0.0	0.0	0.0	0.01	0.0	0.0
(A_r&B_r)	0.0	0.0	0.0	0.0	0.18	0.01
AB_r	0.0	0.0	0.0	0.0	0.2	0.96

Table 2.29 M^{B}. Filtered transition matrix for wells treated with antibiotic B.

$\phi(\hat{T})$ \ $\phi(T)$	U	S	A_r	B_r	$(A_r\&B_r)$	AB_r
U	1.0	0.8	0.64	0.01	0.03	0.02
S	0.0	0.2	0.18	0.0	0.0	0.0
A_r	0.0	0.0	0.18	0.0	0.0	0.0
B_r	0.0	0.0	0.0	0.99	0.21	0.0
(A_r&B_r)	0.0	0.0	0.0	0.0	0.03	0.0
AB_r	0.0	0.0	0.0	0.0	0.73	0.98

Table 2.30 M^{AB}. Filtered transition matrix for wells treated with antibiotic AB.

$\phi(\hat{T})$ \ $\phi(T)$	U	S	A_r	B_r	$(A_r\&B_r)$	AB_r
U	1.0	0.9	0.49	0.98	1.0	0.02
S	0.0	0.1	0.32	0.02	0.0	0.0
A_r	0.0	0.0	0.19	0.0	0.0	0.0
B_r	0.0	0.0	0.0	0.0	0.0	0.0
(A_r&B_r)	0.0	0.0	0.0	0.0	0.0	0.0
AB_r	0.0	0.0	0.0	0.0	0.0	0.98

Table 2.31 M_1^{none}. Filtered transition matrix for the first time point in untreated wells.

$\phi(\hat{T})$ \ $\phi(T)$	U	S	A_r	B_r	$(A_r\&B_r)$	AB_r
U	1.0	0.0	0.0	0.0	0.0	0.0
S	0.0	1.0	0.0	0.0	0.0	0.0
A_r	0.0	0.0	1.0	0.0	0.0	0.0
B_r	0.0	0.0	0.0	1.0	0.17	0.0
(A_r&B_r)	0.0	0.0	0.0	0.0	0.02	0.0
AB_r	0.0	0.0	0.0	0.0	0.81	1.0

Table 2.32 M_1^{A}. Filtered transition matrix for the first time point in wells treated with antibiotic A.

$\phi(\hat{T})$ \ $\phi(T)$	U	S	A_r	B_r	$(A_r\&B_r)$	AB_r
U	1.0	0.98	0.0	0.99	0.23	0.0
S	0.0	0.02	0.0	0.01	0.0	0.0
A_r	0.0	0.0	1.0	0.0	0.54	0.0
B_r	0.0	0.0	0.0	0.0	0.0	0.0
(A_r&B_r)	0.0	0.0	0.0	0.0	0.11	0.0
AB_r	0.0	0.0	0.0	0.0	0.12	1.0

Table 2.33 M_1^{B}. Filtered transition matrix for the first time point in wells treated with antibiotic B.

$\phi(\hat{T})$ \ $\phi(T)$	U	S	A_r	B_r	$(A_r\&B_r)$	AB_r
U	1.0	0.48	0.51	0.02	0.01	0.0
S	0.0	0.52	0.21	0.01	0.0	0.0
A_r	0.0	0.0	0.28	0.0	0.0	0.0
B_r	0.0	0.0	0.0	0.97	0.31	0.0
(A_r&B_r)	0.0	0.0	0.0	0.0	0.1	0.0
AB_r	0.0	0.0	0.0	0.0	0.58	1.0

Table 2.34 M_1^{AB}. Filtered transition matrix for the first time point in wells treated with antibiotic AB.

$\phi(\hat{T})$ \ $\phi(T)$	U	S	A_r	B_r	$(A_r\&B_r)$	AB_r
U	1.0	0.79	0.32	0.67	0.24	0.0
S	0.0	0.21	0.21	0.24	0.21	0.0
A_r	0.0	0.0	0.47	0.0	0.41	0.0
B_r	0.0	0.0	0.0	0.09	0.02	0.0
(A_r&B_r)	0.0	0.0	0.0	0.0	0.07	0.0
AB_r	0.0	0.0	0.0	0.0	0.05	1.0

Table 2.35 Prevention scenario: Effect of treatment strategies on the frequency of uninfecteds (ANOVA).

	Sum of Squares	df	Mean Square	F	Sig.
Between Groups	2.833	5	0.567	779.436	< 0.001
Within Groups	0.013	18	< 0.001		
Total	2.846	23			

Table 2.36 Prevention scenario: Multiple comparison between the effects of treatment strategies on the frequencies of uninfecteds using Tukey's post-hoc analysis.

group1	group2	meandiff	p-adj	lower	upper	reject
Combination	Cycling	-0.027	0.729	-0.087	0.034	False
Combination	Mixing	-0.041	0.317	-0.101	0.020	False
Combination	Mono A	-0.525	0.000	-0.586	-0.465	True
Combination	Mono B	-0.360	0.000	-0.421	-0.300	True
Combination	No treatment	-0.951	0.000	-1.011	-0.890	True
Cycling	Mixing	-0.014	0.975	-0.074	0.047	False
Cycling	Mono A	-0.499	0.000	-0.559	-0.438	True
Cycling	Mono B	-0.334	0.000	-0.394	-0.273	True
Cycling	No treatment	-0.924	0.000	-0.985	-0.864	True
Mixing	Mono A	-0.485	0.000	-0.545	-0.424	True
Mixing	Mono B	-0.320	0.000	-0.380	-0.259	True
Mixing	No treatment	-0.910	0.000	-0.971	-0.850	True
Mono A	Mono B	0.165	0.000	0.104	0.226	True
Mono A	No treatment	-0.425	0.000	-0.486	-0.365	True
Mono B	No treatment	-0.590	0.000	-0.651	-0.530	True

Table 2.37 Prevention scenario: Effect of treatment strategies on the frequency of single resistance (ANOVA).

	Sum of Squares	df	Mean Square	F	Sig.
Between Groups	1.133	5	0.227	290.494	< 0.001
Within Groups	0.014	18	< 0.001		
Total	1.147	23			

Table 2.38 Prevention scenario: Multiple comparison between the effects of treatment strategies on the frequencies of single resistance using Tukey's post-hoc analysis.

group1	group2	meandiff	p-adj	lower	upper	reject
Combination	Cycling	0.030	0.659	-0.033	0.093	False
Combination	Mixing	0.035	0.518	-0.028	0.097	False
Combination	Mono A	0.501	0.000	0.438	0.563	True
Combination	Mono B	0.359	0.000	0.296	0.422	True
Combination	No treatment	0.479	0.000	0.417	0.542	True
Cycling	Mixing	0.005	1.000	-0.058	0.067	False
Cycling	Mono A	0.471	0.000	0.408	0.533	True
Cycling	Mono B	0.329	0.000	0.266	0.392	True
Cycling	No treatment	0.450	0.000	0.387	0.512	True
Mixing	Mono A	0.466	0.000	0.403	0.529	True
Mixing	Mono B	0.325	0.000	0.262	0.387	True
Mixing	No treatment	0.445	0.000	0.382	0.508	True
Mono A	Mono B	-0.142	0.000	-0.204	-0.079	True
Mono A	No treatment	-0.021	0.884	-0.084	0.042	False
Mono B	No treatment	0.120	0.000	0.058	0.183	True

Table 2.39 Prevention scenario: Effect of treatment strategies on the frequency of double resistance (ANOVA).

	Sum of Squares	df	Mean Square	F	Sig.
Between Groups	0.061	5	0.012	157.486	**< 0.001**
Within Groups	0.001	18	**< 0.001**		
Total	0.063	23			

Table 2.40 Prevention scenario: Effect of treatment strategies on the frequency of double resistance (ANOVA).

group1	group2	meandiff	p-adj	lower	upper	reject
Combination	Cycling	0.000	1.000	-0.020	0.020	False
Combination	Mixing	0.003	0.998	-0.017	0.022	False
Combination	Mono A	0.002	1.000	-0.018	0.022	False
Combination	Mono B	0.000	1.000	-0.020	0.020	False
Combination	No treatment	0.136	0.000	0.117	0.156	True
Cycling	Mixing	0.003	0.998	-0.017	0.022	False
Cycling	Mono A	0.002	1.000	-0.018	0.022	False
Cycling	Mono B	0.000	1.000	-0.020	0.020	False
Cycling	No treatment	0.136	0.000	0.117	0.156	True
Mixing	Mono A	-0.001	1.000	-0.021	0.019	False
Mixing	Mono B	-0.003	0.998	-0.022	0.017	False
Mixing	No treatment	0.134	0.000	0.114	0.153	True
Mono A	Mono B	-0.002	1.000	-0.022	0.018	False
Mono A	No treatment	0.134	0.000	0.115	0.154	True
Mono B	No treatment	0.136	0.000	0.117	0.156	True

Table 2.41 Containment scenario: Effect of treatment strategies on the frequency of uninfecteds (ANOVA).

	Sum of Squares	df	Mean Square	F	Sig.
Between Groups	0.639	5	0.128	28.906	**< 0.001**
Within Groups	0.080	18	0.004		
Total	0.718	23			

Table 2.42 Containment scenario: Multiple comparison between the effects of treatment strategies on the frequencies of uninfecteds using Tukey's post-hoc analysis.

group1	group2	meandiff	p-adj	lower	upper	reject
Combination	Cycling	-0.008	1.000	-0.157	0.141	False
Combination	Mixing	-0.041	0.951	-0.190	0.109	False
Combination	Mono A	-0.104	0.282	-0.253	0.046	False
Combination	Mono B	-0.158	0.034	-0.308	-0.009	True
Combination	No treatment	-0.474	0.000	-0.623	-0.325	True
Cycling	Mixing	-0.033	0.980	-0.182	0.117	False
Cycling	Mono A	-0.096	0.361	-0.245	0.054	False
Cycling	Mono B	-0.150	0.048	-0.300	-0.001	True
Cycling	No treatment	-0.466	0.000	-0.616	-0.317	True
Mixing	Mono A	-0.063	0.758	-0.212	0.086	False
Mixing	Mono B	-0.118	0.175	-0.267	0.032	False
Mixing	No treatment	-0.433	0.000	-0.583	-0.284	True
Mono A	Mono B	-0.054	0.850	-0.204	0.095	False
Mono A	No treatment	-0.370	0.000	-0.520	-0.221	True
Mono B	No treatment	-0.316	0.000	-0.465	-0.166	True

Table 2.43 Containment scenario: Effect of treatment strategies on the frequency of single resistance (ANOVA).

	Sum of Squares	df	Mean Square	F	Sig.
Between Groups	0.129	5	0.026	40.881	**< 0.001**
Within Groups	0.011	18	**< 0.001**		
Total	0.140	23			

Table 2.44 Containment scenario: Multiple comparison between the effects of treatment strategies on the frequencies of single resistance using Tukey's post-hoc analysis.

group1	group2	meandiff	p-adj	lower	upper	reject
Combination	Cycling	0.019	0.895	-0.038	0.075	False
Combination	Mixing	0.054	0.067	-0.003	0.110	False
Combination	Mono A	0.197	0.000	0.140	0.253	True
Combination	Mono B	0.102	0.000	0.045	0.158	True
Combination	No treatment	0.169	0.000	0.112	0.225	True
Cycling	Mixing	0.035	0.389	-0.021	0.092	False
Cycling	Mono A	0.178	0.000	0.122	0.235	True
Cycling	Mono B	0.083	0.002	0.027	0.140	True
Cycling	No treatment	0.150	0.000	0.094	0.207	True
Mixing	Mono A	0.143	0.000	0.086	0.199	True
Mixing	Mono B	0.048	0.125	-0.009	0.104	False
Mixing	No treatment	0.115	0.000	0.059	0.172	True
Mono A	Mono B	-0.095	0.001	-0.152	-0.039	True
Mono A	No treatment	-0.028	0.626	-0.084	0.029	False
Mono B	No treatment	0.067	0.015	0.011	0.124	True

Table 2.45 Containment scenario: Effect of treatment strategies on the frequency of double resistance (ANOVA).

	Sum of Squares	df	Mean Square	F	Sig.
Between Groups	0.038	5	0.008	1.169	0.362
Within Groups	0.116	18	0.006		
Total	0.154	23			

Table 2.46 Maximum-emergence scenario: Effect of treatment strategies on the frequency of uninfecteds (ANOVA).

	Sum of Squares	df	Mean Square	F	Sig.
Between Groups	1.432	5	0.286	383.054	**< 0.001**
Within Groups	0.013	18	**< 0.001**		
Total	1.445	23			

Table 2.47 Maximum-emergence scenario: Multiple comparison between the effects of treatment strategies on the frequencies of uninfecteds using Tukey's post-hoc analysis.

group1	group2	meandiff	p-adj	lower	upper	reject
Combination	Cycling	-0.306	0.000	-0.368	-0.245	True
Combination	Mixing	-0.386	0.000	-0.447	-0.324	True
Combination	Mono A	-0.414	0.000	-0.476	-0.353	True
Combination	Mono B	-0.499	0.000	-0.561	-0.438	True
Combination	No treatment	-0.823	0.000	-0.885	-0.762	True
Cycling	Mixing	-0.079	0.008	-0.141	-0.018	True
Cycling	Mono A	-0.108	0.000	-0.169	-0.046	True
Cycling	Mono B	-0.193	0.000	-0.254	-0.131	True
Cycling	No treatment	-0.517	0.000	-0.578	-0.455	True
Mixing	Mono A	-0.029	0.681	-0.090	0.033	False
Mixing	Mono B	-0.114	0.000	-0.175	-0.052	True
Mixing	No treatment	-0.438	0.000	-0.499	-0.376	True
Mono A	Mono B	-0.085	0.004	-0.146	-0.024	True
Mono A	No treatment	-0.409	0.000	-0.470	-0.347	True
Mono B	No treatment	-0.324	0.000	-0.385	-0.262	True

Table 2.48 Maximum-emergence scenario: Effect of treatment strategies on the frequency of single resistance (ANOVA).

	Sum of Squares	df	Mean Square	F	Sig.
Between Groups	1.311	5	0.262	524.241	**< 0.001**
Within Groups	0.009	18	**< 0.001**		
Total	1.320	23			

Table 2.49 Maximum-emergence scenario: Multiple comparison between the effects of treatment strategies on the frequencies of single resistance using Tukey's post-hoc analysis.

group1	group2	meandiff	p-adj	lower	upper	reject
Combination	Cycling	0.342	0.000	0.292	0.393	True
Combination	Mixing	0.408	0.000	0.358	0.459	True
Combination	Mono A	0.549	0.000	0.499	0.600	True
Combination	Mono B	0.536	0.000	0.486	0.586	True
Combination	No treatment	0.761	0.000	0.710	0.811	True
Cycling	Mixing	0.066	0.006	0.016	0.116	True
Cycling	Mono A	0.207	0.000	0.157	0.257	True
Cycling	Mono B	0.194	0.000	0.143	0.244	True
Cycling	No treatment	0.418	0.000	0.368	0.469	True
Mixing	Mono A	0.141	0.000	0.091	0.191	True
Mixing	Mono B	0.128	0.000	0.077	0.178	True
Mixing	No treatment	0.352	0.000	0.302	0.403	True
Mono A	Mono B	-0.013	0.956	-0.064	0.037	False
Mono A	No treatment	0.211	0.000	0.161	0.262	True
Mono B	No treatment	0.225	0.000	0.174	0.275	True

Table 2.50 Maximum-emergence scenario: Effect of treatment strategies on the frequency of double resistance (ANOVA).

	Sum of Squares	df	Mean Square	F	Sig.
Between Groups	0.109	5	0.022	71.779	**< 0.001**
Within Groups	0.005	18	**< 0.001**		
Total	0.115	23			

Table 2.51 Maximum-emergence scenario: Effect of treatment strategies on the frequency of double resistance (ANOVA).

group1	group2	meandiff	p-adj	lower	upper	reject
Combination	Cycling	0.058	0.002	0.019	0.097	True
Combination	Mixing	0.071	0.000	0.032	0.110	True
Combination	Mono A	0.009	0.980	-0.031	0.048	False
Combination	Mono B	0.069	0.000	0.030	0.108	True
Combination	No treatment	0.206	0.000	0.167	0.245	True
Cycling	Mixing	0.013	0.884	-0.026	0.052	False
Cycling	Mono A	-0.049	0.009	-0.088	-0.010	True
Cycling	Mono B	0.011	0.937	-0.028	0.051	False
Cycling	No treatment	0.148	0.000	0.109	0.188	True
Mixing	Mono A	-0.062	0.001	-0.102	-0.023	True
Mixing	Mono B	-0.002	1.000	-0.041	0.037	False
Mixing	No treatment	0.135	0.000	0.096	0.174	True
Mono A	Mono B	0.060	0.001	0.021	0.100	True
Mono A	No treatment	0.198	0.000	0.158	0.237	True
Mono B	No treatment	0.137	0.000	0.098	0.176	True

Table 2.52 Maximum-emergence scenario: Effect of treatment strategies on the frequency of newly emerging double resistance (ANOVA).

	Sum of Squares	df	Mean Square	F	Sig.
Between Groups	0.035	5	0.007	41.272	**< 0.001**
Within Groups	0.010	60	**< 0.001**		
Total	0.045	65			

Table 2.53 Maximum-emergence scenario: Multiple comparison between the effects of treatment strategies on the frequencies of newly emerging double resistance using Tukey's post-hoc analysis.

group1	group2	meandiff	p-adj	lower	upper	reject
Combination	Cycling	0.013	0.227	-0.004	0.029	False
Combination	Mixing	0.021	0.004	0.005	0.038	True
Combination	Mono A	0.003	0.990	-0.013	0.020	False
Combination	Mono B	0.024	0.001	0.008	0.041	True
Combination	No treatment	0.070	0.000	0.053	0.086	True
Cycling	Mixing	0.009	0.597	-0.007	0.025	False
Cycling	Mono A	-0.009	0.569	-0.026	0.007	False
Cycling	Mono B	0.012	0.308	-0.005	0.028	False
Cycling	No treatment	0.057	0.000	0.041	0.073	True
Mixing	Mono A	-0.018	0.022	-0.035	-0.002	True
Mixing	Mono B	0.003	0.997	-0.014	0.019	False
Mixing	No treatment	0.048	0.000	0.032	0.065	True
Mono A	Mono B	0.021	0.005	0.004	0.037	True
Mono A	No treatment	0.066	0.000	0.050	0.083	True
Mono B	No treatment	0.045	0.000	0.029	0.062	True

Table 2.54 Maximum-emergence scenario: Effect of treatment strategies on the frequency of super-infections (ANOVA).

	Sum of Squares	df	Mean Square	F	Sig.
Between Groups	0.019	5	0.004	11.731	**< 0.001**
Within Groups	0.017	52	**< 0.001**		
Total	0.036	57			

Table 2.55 Maximum-emergence scenario: Multiple comparison between the effects of treatment strategies on the frequencies of superinfections using Tukey's post-hoc analysis.

group1	group2	meandiff	p-adj	lower	upper	reject
Combination	Cycling	0.024	0.202	-0.007	0.055	False
Combination	Mixing	0.036	0.015	0.005	0.067	True
Combination	Mono A	0.035	0.021	0.004	0.066	True
Combination	Mono B	0.026	0.160	-0.005	0.057	False
Combination	No treatment	0.068	0.000	0.037	0.099	True
Cycling	Mixing	0.011	0.674	-0.011	0.034	False
Cycling	Mono A	0.010	0.768	-0.013	0.033	False
Cycling	Mono B	0.002	1.000	-0.022	0.025	False
Cycling	No treatment	0.043	0.000	0.021	0.066	True
Mixing	Mono A	-0.001	1.000	-0.024	0.021	False
Mixing	Mono B	-0.010	0.810	-0.033	0.013	False
Mixing	No treatment	0.032	0.001	0.009	0.055	True
Mono A	Mono B	-0.009	0.881	-0.032	0.015	False
Mono A	No treatment	0.033	0.001	0.011	0.056	True
Mono B	No treatment	0.042	0.000	0.019	0.065	True

Table 2.56 Maximum-emergence scenario: Effect of drug ϑ on the frequency of emergence per superinfection (ANOVA).

	Sum of Squares	df	Mean Square	F	Sig.
Between Groups	10.194	3	3.398	143.661	**< 0.001**
Within Groups	1.443	61	0.024		
Total	11.637	64			

Table 2.57 Maximum-emergence scenario: Multiple comparison between the effects of drug ϑ on the frequencies of emergence per superinfection using Tukey's post-hoc analysis.

group1	group2	meandiff	p-adj	lower	upper	reject
A	AB	-0.082	0.752	-0.300	0.136	False
A	B	0.740	0.000	0.624	0.855	True
A	none	0.857	0.000	0.711	1.002	True
AB	B	0.822	0.000	0.602	1.042	True
AB	none	0.939	0.000	0.701	1.176	True
B	none	0.117	0.174	-0.032	0.266	False

Bibliography

[1] .S. Tschudin-Sutter, R. Frei, F. Schwahn, M. Tomic, M. Conzelmann, A. Stranden, and A. F. Widmer. "Prospective validation of cessation of contact precautions for extended-spectrum β-lactamase-producing Escherichia coli1". In: Emerg. Infect. Dis. 22.6 (2016), pp. 1094–1097. issn: 10806059. doi: 10.3201/eid2206.150554.

[2] .J. S. Huisman, T. G. Vaughan, A. Egli, S. Tschudin-Sutter, T. Stadler, and S. Bonhoeffer. "The effect of sequencing and assembly on the inference of horizontal gene transfer on chromosomal and plasmid phylogenies". In: Philos. Trans. R. Soc. B Biol. Sci. 377.1861 (2022). issn: 14712970. doi: 10.1098/rstb.2021.0245.

[3] .T. Fehér, B. Bogos, O. Méhi, G. Fekete, B. Csörg, K. Kovács, G. Pósfai, B. Papp, L. D. Hurst, and C. Pál. "Competition between transposable elements and mutator genes in bacteria". In: Mol. Biol. Evol. 29 (2012), pp. 3153–3159. issn: 0737-4038. doi: 10.1093/molbev/mss122.

[4] .A. Carattoli, A. Bertini, L. Villa, V. Falbo, K. L. Hopkins, and E. J. Threlfall. "Identification of plasmids by PCR-based replicon typing". In: J. Microbiol. Methods 63.3 (2005), pp. 219–228. issn: 01677012. doi: 10.1016/j.mimet.2005.03.018.

[5] .J. S. Huisman, F. Benz, S. J. Duxbury, J. A. G. de Visser, A. R. Hall, E. A. Fischer, and S. Bonhoeffer. "Estimating plasmid conjugation rates: A new computational tool and a critical comparison of methods". In: Plasmid 121.September 2021 (2022), p. 102627. issn: 10959890. doi: 10.1016/j.plasmid.2022.102627. url: https://doi.org/10.1016/j.plasmid.2022.102627.

[6] .P. Virtanen et al. "SciPy 1.0: fundamental algorithms for scientific computing in Python". In: Nat. Methods 17.3 (2020), pp. 261–272. issn: 15487105. doi: 10.1038/s41592-019-0686-2. arXiv: 1907.10121.

[7] .S. Seabold and J. Perktold. "Statsmodels: Econometric and Statistical Modeling with Python". In: Proc. 9th Python Sci. Conf. 2010, pp. 92–96. doi: 10.25080/majora-92bf1922-011.

[8] .J. E. Cates, R. Christie, and L. P. Garrod. "Penicillin-resistant subacute bacterial endocarditis treated by a combination of penicillin and streptomycin". In: Br. Med. J. 31.11 (1951), pp. 1120–1120. doi: 10.1136/bmj.1.4708.653.

[9] .E. Jawetz, J. B. Gunisson, and V. R. Coleman. "Observations on the mode of action of Synergism and Antagonism". In: Antibiot. Annu. 5 (1954), pp. 520–528. issn: 05703131.

[10] .P. S. Ocampo, V. Lázár, B. Papp, M. Arnoldini, P. A. Zur Wiesch, R. Busa-Fekete, G. Fekete, C. Pál, M. Ackermann, and S. Bonhoeffer. "Antagonism between bacteriostatic and bactericidal antibiotics is prevalent". In: Antimicrob. Agents Chemother. 58.8 (2014), pp. 4573–4582. issn: 1098-6596. doi: 10.1128/AAC.02463-14.

[11] .S. A. Angermayr, T. Y. Pang, G. Chevereau, K. Mitosch, M. J. Lercher, and T. Bollenbach. "Growth-mediated negative feedback shapes quantitative antibiotic response". In: Mol. Syst. Biol. 18.9 (2022), pp. 1–19. issn: 1744-4292. doi: 10.15252/msb.202110490.

Concluding Remarks

3

3.1 Is combination the best treatment strategy?

3.2 Can we use change of luminescent light intensity to approximate the net growth rate?

3.3 can we extrapolate sub-mic measures of drug interactions to the super-mic?

3.4 General Concluding Note

Bibliography